ISSN 2347 - 3037

Indian Journal of Tribology

Volume 7 Number 1 July 2016

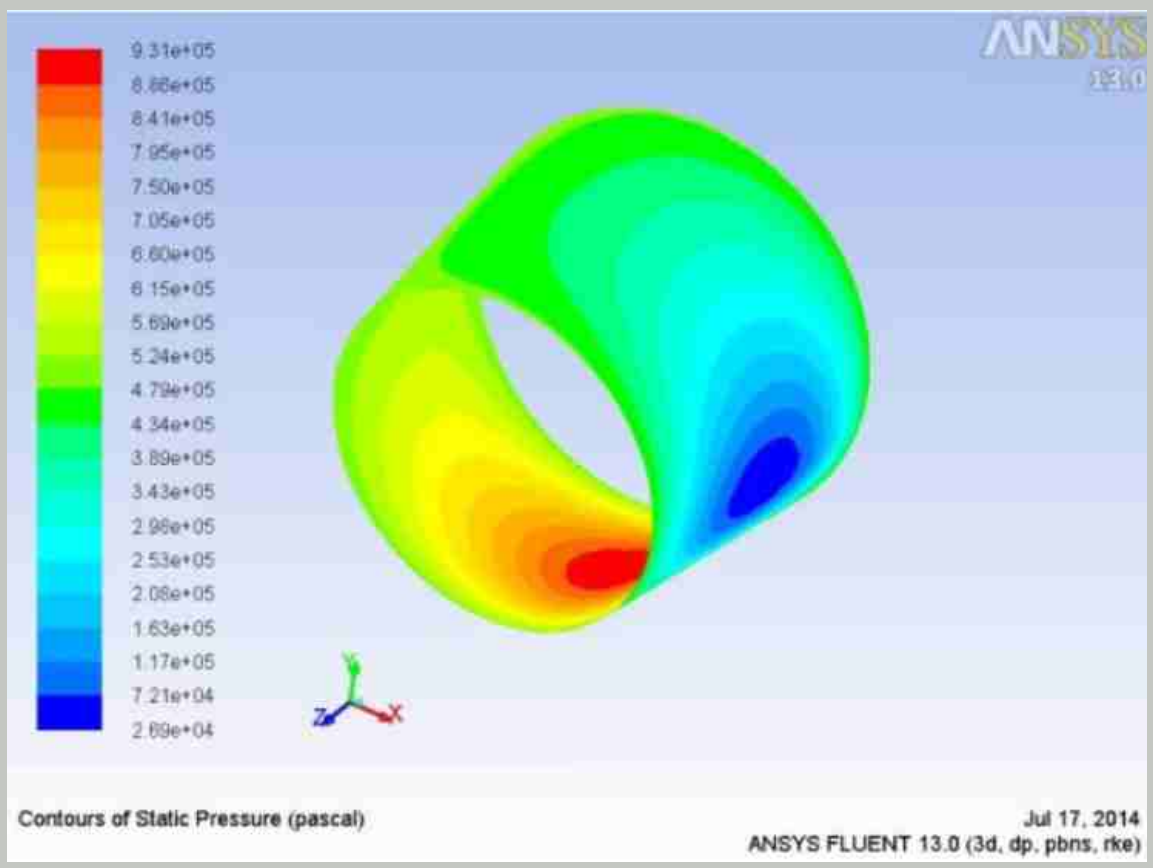

Editorial Board

Printed on Behalf of the
Tribology Society of India
(Affiliated the the International Tribology Council (UK))
C/o. Indian Oil Corporation Ltd.
R&D Centre, Sector-13., Faridabad. HARYANA
Phone no: +91-129-2294264
E-mail : info@tribologyindia.org

Indian Journal of Tribology
ISSN 2347 - 3037
Vol. 1, No. 1, September 2015

Contents

Associate Editor's Message

My Greetings to All

I am happy to be a part of Editorial process of this issue of Indian Journal of Tribology.

This issue contains contributions by authors related to tribology of hybrid composites, bearings, FEM approach in solving tribological problems, tribology of innovatively formed light weight materials.

On behalf of the editorial board, I urge all the Tribologists both in India and abroad from academic institutions as well as industries to contribute their research and practical solutions in form of case studies for publication in this journal.

I am happy to share with all the readers that this journal is gaining popularity among both practicing tribologists as well as academic circles.

Wishing All the Readers a Wonderful Time

Dr. C. S. Ramesh
Associate Editor
Dean, School of Engineering
Dayananda Sagar University, Bangalore

3D INVESTIGATION ON AIR JET ERODED SURFACES OF AL-ALLOY AND ITS COMPOSITE

Shreeshail M. L.[1*] and Harsha R. Gudi[2]

[1]Department of Mechanical Engineering, B.V. Bhoomaraddi College of Engineering and Technology, Hubli, Karnataka-580031, India.
[2]Department of Mechanical Engineering, BMS College of Engineering, Bangalore, India.
*Corresponding author (E-mail: shreeshailmlmech@yahoo.com)

KEY WORDS: MMC's ; Al6061 ; SiC ; Erosion ; Surface morphology.

ABSTRACT

The usual surface failures of engineering materials due to wear-erosion, fatigue are drawing a major concern on the surface life, structural behavior and its properties. There is a need of extended service life of the engineered materials. The reinforcement of silicon carbide (SiC) particles in the metal matrix composite (MMC's) and their improvement in the hardness of the composite material has proved the resistance to erosion. The surface morphology of air jet eroded Aluminium 6061 alloy and Al6061-SiC-C_f composite material produced by material removal and plastic deformation are investigated. The experimental results of both samples were obtained by ASTM G76 standards using air jet erosion test rig. The investigation is emphasized on different scales with the help of Con-focal microscopy and atomic force microscopy (AFM).

After the erosion test on both samples, Al6061 alloy's weight loss originating from the crater resulted in larger volume of material loss when compared to Al6061-SiC-C_f composite. The key role of SiC particles in the matrix and its resistance to erosion is highlighted in this investigation. The dominance of two mechanisms was found to be contributing factors for the erosion, micro-cracking and nano-ploughing. The considerable improvements in mechanisms on the composite are also discussed.

INTRODUCTION

Processing and characterization of metal matrix composites has already drawn ample attention and today, lot of successful work can be found on different fabricating routes of MMC **[1, 3, 5]**. The expectation from the composite has also increased to deliver the properties which can fit any specified application **[1, 3]**. The MMC's prime function is not only restricted to tolerate any solid particle impact, but also other two different impact forms i.e. gaseous and fluid. Given the different working conditions, the new-age composites have to sustain external forces and deal with different surface challenges **[2]**. These challenges might even extend to extreme conditions such as heat and high velocity impact. Thermal power plants, coal processing plants and gas turbine engines, are some of the major industries which are facing the erosion problem. To overcome this critical erosion problem, the eroded surfaces were examined to analyze wear mechanisms using 3D optical profile scanner **[4]**. Even lots of solutions are examined and suggested, varying from providing coating layer on the metal to the extent of improving the base metal properties **[4, 5]**.

In the present work, the Al6061 alloy and Al6061-SiC-C_f composite are assessed for air jet erosion tests. Our investigation will analyze three dimensional eroded surfaces with the help of conventional SEM study, and unusual confocal-AFM studies. Our study also exposes the wear behavior to nano scale on both the eroded alloy and composite.

EXPERIMENTAL DETAILS

SiC particles and Carbon fibres (C_f) are the reinforcements and Al6061 being the matrix material. With the help of 100T hydraulic press, the powder-fibre mixture was compacted. In a single compact composite mix, the weight percentage of reinforcements i.e. SiC powder and Carbon fibres were 60 and 05 Wt% respectively. The inclusion of carbon fibres (C_f) in the compact mix which is in minimal weight percentage is only an attempt to reduce

Table 1: Air jet erosion Test Conditions

Sl. No.	Test Parameters	
1.	Erodent material	Silica sand
2.	erodent size (mm)	300
3.	Particle velocity (m/s)	30
4.	Erodent feed rate (g/m)	2
5.	Impact angle (degrees)	90 and 45
6.	Test temperature	Room temperature
7.	Test duration (minutes)	30 (in steps of 5)
8.	Sample size (mm)	25x25x8
9.	Standoff distance (mm)	10
10.	System pressure (bar)	1.4

total composite weight. Molten Al6061 alloy was poured into the mould, inside which the composite mix compacts were arranged in a circular manner. The same casted billets were hot extruded using 200T hydraulic press adopting an extrusion ratio of 1:4 and an extrusion temperature of 520°C. This hot extruded composite was subjected to dry air jet erosion wear tests. The test conditions are shown in the table 1. Weight of both hot extruded Al6061 alloy and Al6061-SiC-C_f composite before and after erosion wear tests were recorded using a precision micro balance of accuracy 0.1 mg.

RESULTS

For both the test samples, the weight loss at 45° impact angle is more when compared to normal impact angle of 90°. The figure 1 shows the graph of test duration with erosion weight loss.

At 45° impact, the Al-alloy shows comparatively more material loss due to the easy plastic deformation and material removal. While the composite exhibits the resistance to erosion for both the impact angle.

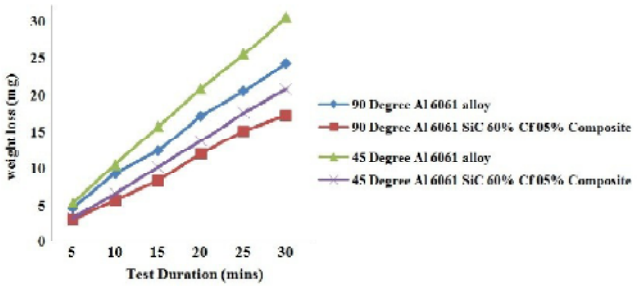

Fig. 1: Variation of weight loss of Al6061 alloy and Al6061-SiC-C_f composite at two different impact angles.

DISCUSSION

Surface morphology of air jet eroded surfaces has been discussed. In Scanning Electron Microscopy (SEM) studies, Figure 2 to Figure 5 shows the erosion mechanism. The easy flow-metal cutting is more on the alloy surface than that of the composites'. The presence of SiC particles in the matrix withstands the erosion wear.

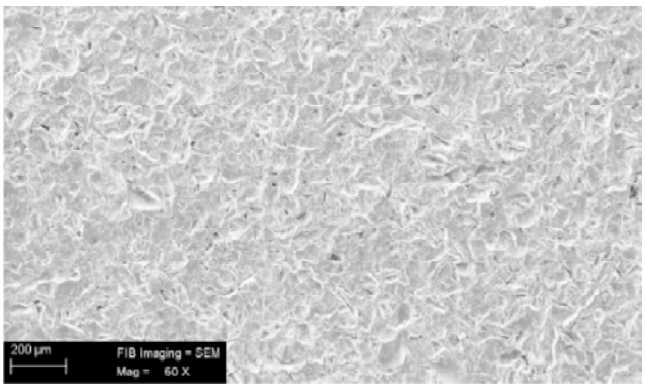

***Fig. 2:** SEM of 90 degree impact on Al 6061 alloy.*

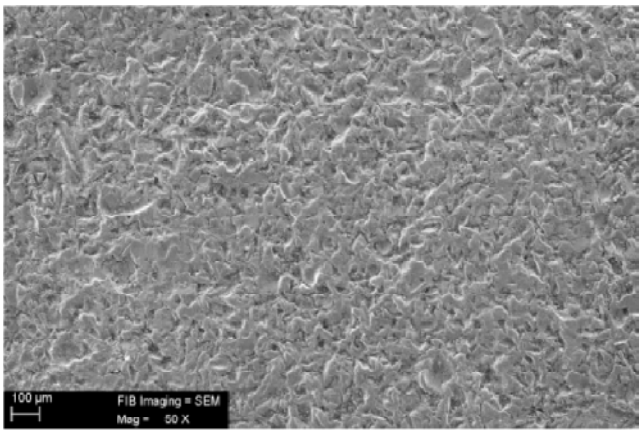

Fig. 3: SEM of 90 degree impact on Al 6061 60% SiC 05% C_f Composite

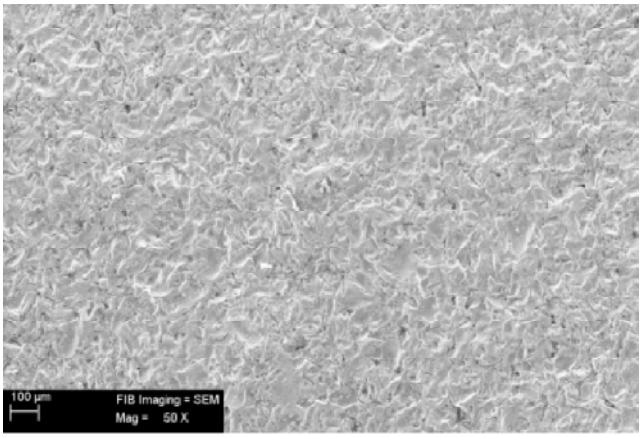

Fig. 4: SEM of 45 degree impact on Al 6061 alloy.

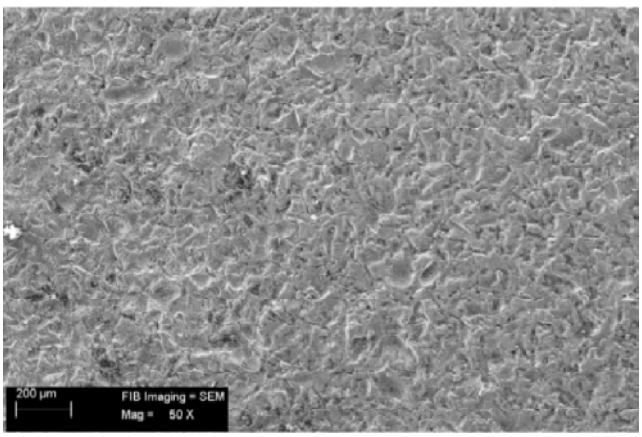

Fig. 5: SEM of 45 degree impact on Al 6061 60% SiC 05% C_f Composite.

In Confocal Studies, Figure 6 and Figure 7 compares the eroded surface profiles up to micro scale to get the extreme eroded depth (cross-sectional) of 390 µm and 334 µm at 90° and 489 µm and 145 µm at 45° for alloy and composites respectively. The AFM study reveals the wear mechanism on both micro and nano scales. Figure 8 to Figure 11 shows the mechanism with the eroded cross-

sectional depth of 4 µm and 750 nm for alloy and 1.8 µm and 500 nm for composite at 90° and 45° impact respectively.

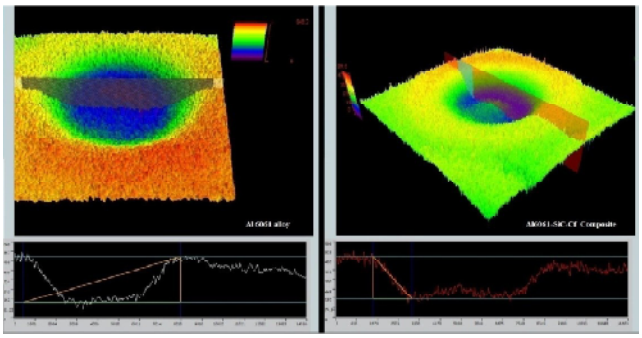

Fig. 6: Confocal Microscopy comparing 90 degree impact surfaces of Al 6061 alloy and Al 6061 60% SiC 05% C_f Composite.

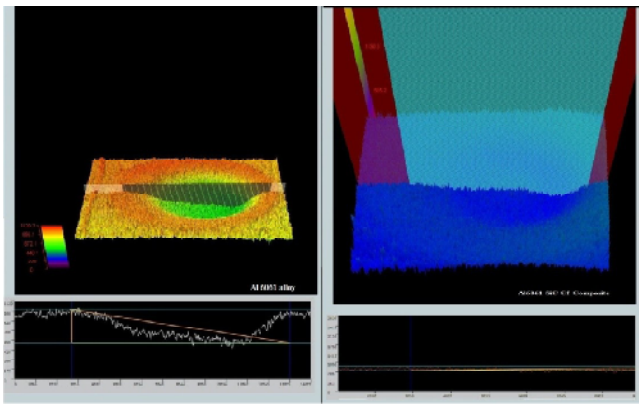

Fig. 7: Confocal Microscopy comparing 45 degree impact surfaces of Al 6061 alloy and Al 6061 60% SiC 05% C_f Composite.

Both the Confocal and AFM studies leads us to two things, first, 90° impact creates only crates of micro scale (micro-cracking) while second, the 45° impact creates lengthy sweep called as ploughing of material (micro-ploughing) on the surface of up to nano scale.

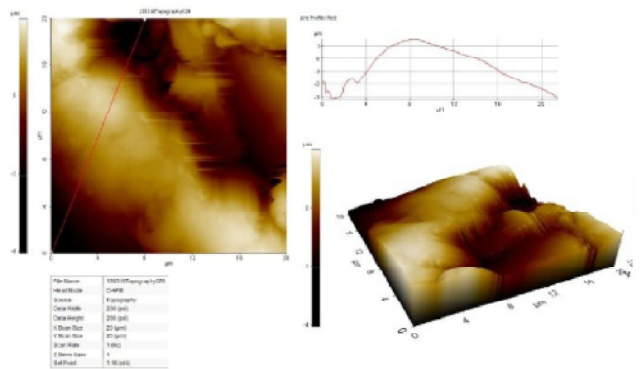

Fig. 8: AFM of 90 degree impact on Al 6061 alloy.

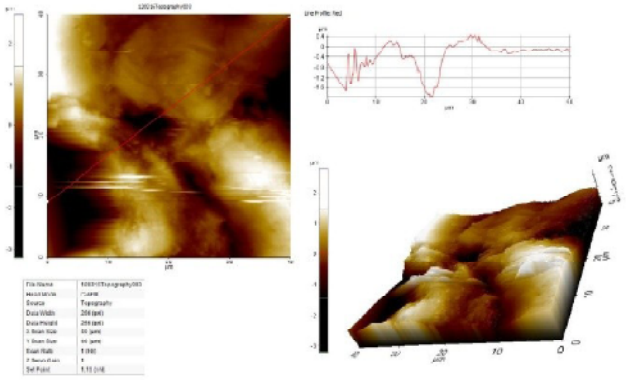

Fig. 9: AFM of 90 degree impact on Al 6061 60% SiC 05% C_f Composite.

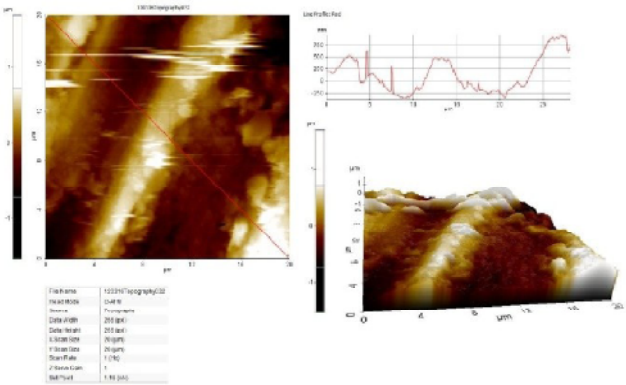

Fig. 10: AFM of 45 degree impact on Al 6061 alloy.

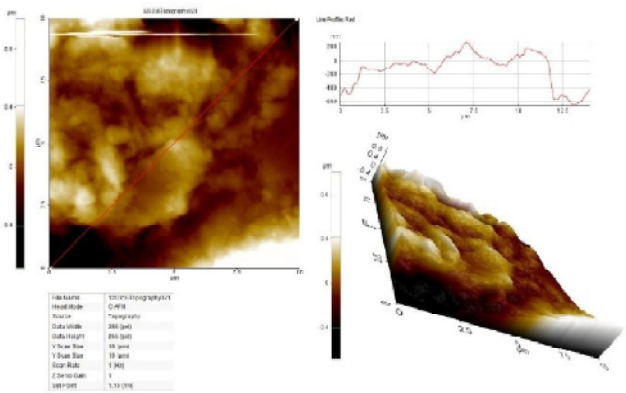

Fig. 11: AFM of 45 degree impact on Al 6061 60% SiC 05% C_f Composite.

CONCLUSIONS

- Three dimensional eroded surface studies of both Al6061 alloy and its composite not only indicate the dominance of micro-cracking, micro-ploughing mechanism, it also reveals the fluctuation of erosion from micro to nano scale.

- This investigation exposes erosion-wear resistance and therefore an extended service life of Al6061-SiC-C_f composite compared to Al6061 alloy.

ACKNOWLEDGEMENTS

The authors would like to thank Prof D. Jawahar, C.E.O, P.E.S Group of Institutions for the encouragement. We would like to thank Dr K.N.B Murthy, Principal & Director, Dr. K.S. Sridhar, Head of Department, Mechanical Engineering, P.E.S University for their encouragement and support. We would like to extend our thanks to Prof. L. Krishnamurthy, Head, CNT lab, for the facilities at NIE, Mysore-08.

REFERENCES

1. R.K. Uyyuru, M.K. Surappa, and S. Brusethaug, Tribological behavior of Al–Si–SiCp composites/ automobile brake pad system under dry sliding conditions. Tribology International, 2007, Vol. **40**, pp. 365–373.
2. Ranjit Bauri and M.K. Surappa, Sliding wear behavior of Al–Li–SiCp composites. Wear, 2008, Vol. **265**, pp. 1756–1766.
3. Ramesh. C. S, Harsha. R. Gudi, Nirupama Mohan and Adarsh. H, Development of innovative Al6061-SiC composite by hybrid technique. Editors- *Proceedings of STLE 2012 Conference*, St. Louis, USA, May 6-10, 2012.
4. M. R. Ramesh, S. Prakash, S. K. Nath, Pawan Kumar Sapra, B. Venkataraman, Solid Particle erosion of HVOF sprayed WC-Co/NiCrFeSiB coatings, Wear, 2010, Vol. **269**, pp. 197-205.
5. Amar Patnaik, T.G. Mamatha, Sandhyarani Biswas and Predeep Kumar, Damage assessment of titania filled zinc-aluminum alloy metal matrix composites in erosive environment: A comparative study. Materials and Design, 2012, Vol. **36**, pp. 511-521.

MICROSTRUCTURAL STUDIES OF RCS PROCESSED AA6061 ALLOY SUBJECTED TO DRY SLIDING WEAR TEST

Prabhakar M. Bhovi[1*], K.Venkateswarlu[2]

[1]B.V.B. College of Engineering and Technology, Hubli-580031
[2]CSIR-National Aerospace Laboratories, Bangalore - 560017
*Corresponding author: prabhakar2280@gmail.com

KEYWORDS: 'Dry sliding wear', 'RCS process','AA6061alloy',' SEM', ' Wear resistance'.

ABSTRACT

AA6061 alloy was subjected to repetitive corrugation and straightening (RCS) process. This has been widely accepted as one of the promising method in severe plastic deformation routes. AA 6061 alloy was processed by RCS up to eight passes with rotation 90° and without rotation after each pass. The process includes repetitively bending the sample and straightening as such there was no significant change in the geometry of sample. The process was to introduce large number of dislocations and a result formation of sub grain and high angle grain boundaries. This reduction in grain size would substantially responsible for obtaining improved mechanical and sliding wear properties. As cast and 8 pass samples of AA6061alloy were subjected to dry sliding wear test as per ASTM G99. Applied load, sliding distance on wear rate, during dry sliding wear were studied in detail. The results clearly demonstrated that there is significant reduction grain size after RCS and led to improved hardness values and sliding wear resistance results. Moreover, the rotation after each pass showed a marginal improvement in the hardness and sliding wear results. In addition, as the number of passes is increased, a continuous improvement in hardness and sliding wear resistance is observed. The reduction in grain size and its influence on sliding wear performance is explained in detail through Scanning Electron Microscopy studies. It is concluded that the RCS can be a processing method for obtaining a superior alloy. The sliding wear performance of RCS processed AA 6061 is mostly depend on applied load, grain size and hardness.

INTRODUCTION

Many engineering components fail primarily due to wear and corrosion in aggressive interacting environments. Designing such components for longer life, generally include different approaches. The first approach is bulk material design with high wear resistance and corrosion resistance and second approach is modification of the functional surfaces to work satisfactorily. The third and final approach where the bulk material subjected to severe plastic deformation. This not only improves the strength but also increases the hardness. This finally leads to enhanced in wear resistance properties.

Aluminium and its alloys are extensively used for several applications in the field of automotive and aerospace industries. The main advantage of using aluminium alloys is mainly high strength to weight ratio. Aluminium alloys are available from 1xxx to 8xxx series in which AA6061 alloy is having good castability, formability and weldability **[1- 3]**. The severe plastic deformation is most prominent technique to improve the mechanical properties like strength and hardness. There are several SPD techniques to produce bulk nanostructured materials, including equal channel angular pressing (ECAP) and high-pressure torsion (HPT). In ECAP, it is limited to process samples only up to certain sizes. In HPT, only disk shaped small samples can be processed under pressure and torsional deformation **[4]**. Material loss is the major problem for all the engineering products during its fabrication. As a result, it is always desired to produce materials that have unique properties and research work is carried out for newer materials **[5]**.

In the recent past, many processing methods are developed for fabricating a engineering material that has unique mechanical properties. Among these processing methods, severe plastic deformation (SPD) has been conceded as the cost efficient method to produce ultra-fine and nanostructured materials with improved mechanical properties. In various SPD methods, repetitive corrugation and straightening process is focussed as a novel method for producing ultra-fine grain structured Al alloys with improved mechanical properties and suitable for industrial usage **[6,7,8]**. In this method, a large plastic strain is induced in to the material, leads to reduction in grain size from micrometre to sub micrometre level and formation of sub grain and low angle to high angle grain boundaries **[9]**. Extensive studies have been carried out to understand grain refinement and the effect of grain refinement with other SPD methods to improve mechanical properties of the materials **[10, 11]**.The reduction in grain size would substantially increase in the

hardness and sliding wear properties. Many researchers have reported the effect of sliding wear properties of aluminium based composites **[12]**. Sarkar and Clarke have worked on aluminium-silicon alloys and reported transition wear rate with load applied **[13]**.The mechanism of dry sliding wear in metals and commented that the observed transition from severe to mild wear after defined parameters was attributed to the formation of layer on the wear surface**[14]**.The shear strain increased with the surface of the material removal and cracks appeared on the surface by delaminating phenomenon**[15,16]** Investigations on the development of RCS process on bulk metals or alloys to produce ultrafine grained structures, mechanical, and microstructural characterization, however, have hardly been reported **[17,18,19]**. In this paper we present the effect of RCS process, dry sliding wear test as per ASTM G99 pin on disc to as cast of AA6061 alloy and RCS processed samples after 8 passes could increase the wear resistance of the sample to the applied load and sliding distance and micrograph of worn surfaces observation through scanning electron microscopy.

EXPERIMENTAL PROCEDURE AND MATERIALS

Materials

AA 6061 alloy was chosen to investigate the effect of RCS processing up to 8 pass on wear resistance with as cast AA6061 alloy. The AA6061 alloy composition as shown in the Table1.

AA6061 alloy was homogenised by heating in the furnace at 450°C temperature and then cooled in the furnace about 12 h. In the present study the RCS process is applied to AA6061 alloy of dimension 12×12×125 mm^3 size by 50 ton capacity hydraulic press which has corrugated and straightening die. Specimens were bent in a corrugated die and then straightened in the press. Samples were processed for 1to 8 passes either rotation between passes or by rotating the samples by 90°, each pass is repetitive bent (corrugated) and straightened. The RCS process imparts dynamic recovery and subsequently improves the grain refinement and thereby increase in the hardness. The reduction in grain size would substantially responsible for obtaining improved mechanical and sliding wear property.

Dry sliding wear test

The wear specimens were tested under dry (un-lubricated) condition with ASTM-G99 standards using pin-on-disc sliding wear testing machine (Make: DUCOM). A standard test procedure was employed. Specimens of size 8×8×25 mm were cut from the as cast and RCS processed samples, and then machined and polished. The wear track and RCS processed AA6061 alloy samples are cleaned thoroughly with acetone prior to test. After that the specimen is mounted on the pin holder of the tribometer ready for wear test. During the test, the sample is held pressed against a rotating EN32 steel disc (hardness of 65HRC) by applying load that acts as counter weight and balances the sample. The track diameter was chosen as 80 mm and the parameters such as the load, sliding speed and sliding distance were varied with wear resistance, coefficient of friction and frictional force. Once the surface in contact with disc the specimen wears out, the load pushes the arm to remain in contact with the disc. Test was carried out for as cast AA6061 alloy and RCS processed of AA6061 alloy up to 8 pass. The experimental readings and graphs were obtained with system connected software WINDUCOM.

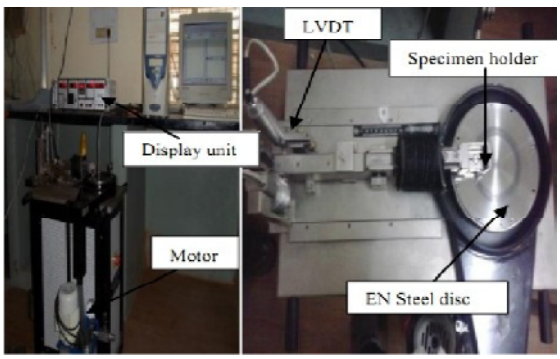

Fig. 1: Experimental setup of pin-on-disc dry sliding wear testing machine

RESULTS AND DISCUSSION

Vickers Hardness test was carried out on RCS processed and as cast samples of AA6061 alloy. The hardness is improved by 3 times compared to as cast. The experiments were conducted as per ASTM-G99 standards and the wear rate results obtained for various combinations of parameters like load applied and sliding distance.

Microhardness studies

Microhardness measurements were taken on AA6061 alloy in as cast condition. Moreover, readings were also taken on RCS processed AA 6061 samples. Two type RCS tests were conducted. The first set consists of without rotation after each pass and the second type was, with 90°rotation between each pass. The mcirohardness results

Table-1 Chemical composition of AA6061 alloy

Element	Mg	Si	Fe	Cu	Zn	Mn	Ti	Cr	Al
Weight %	0.8	0.64	0.23	0.17	0.031	0.072	0.015	0.016	Balance

of the eight RCS passed samples shown in Fig.2. The results clearly demonstrate that the hardness measurements are uniform over a total length of sample. As-cast AA 6061 alloy exhibited hardness value of ~40 VHN. RCS processed samples with rotation and without rotation exhibited hardness values of ~105 VHN and ~120 VHN, respectively. These results suggest that a rotation of sample between passes is beneficial in producing a high level of strain that yielded high hardness values. In addition, the results further suggest that the samples without rotation resulted low hardness values is probably due to the inhomogeneous strain induced in the samples. Moreover, the hardness values are also not uniform throughout the samples suggesting an inhomogeneous distribution of strain in the sample.

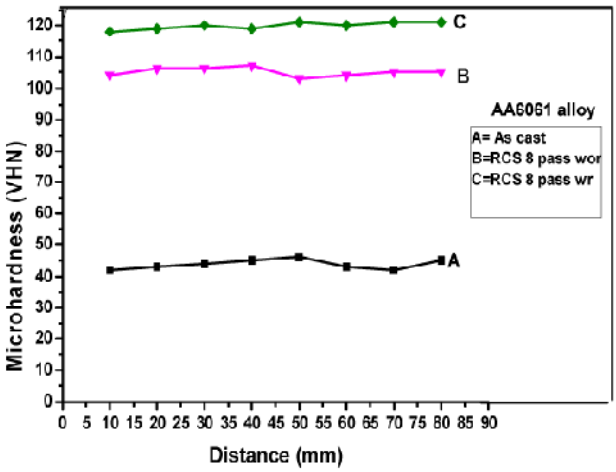

Fig. 2: Microhardeness value variation in the RCS processed AA 6061 alloy

The effect of sliding distance and applied load on the wear rate

The eight pass RCS processed AA6061 alloy shows improved sliding wear resistance results as compared to as cast AA6061 alloy. The effects of both applied load and sliding distance was investigated as a function of the e experimental alloys. Figure 3(a) and 3(b) represents the wear loss of the as cast and RCS processed alloy without rotation up to 8pass to as cast for 5N and 10N testing condition. The graph clearly shows that there is decrease in the wear loss with RCS processed alloy to as cast for applied load and sliding distance.

It is clearly observed from the Fig. 3 (a), (b) that there is a sudden increase in the wear loss of as cast and RCS 8 pass AA 6061 samples at load applied. This is basically adhesion that takes place between the sample surface and surface of counter disk. Further increase in sliding distance was responsible almost and a continuous loo of wear loss as the sliding distance is increased. These results further suggest that at lower sliding distance, the wear loss is

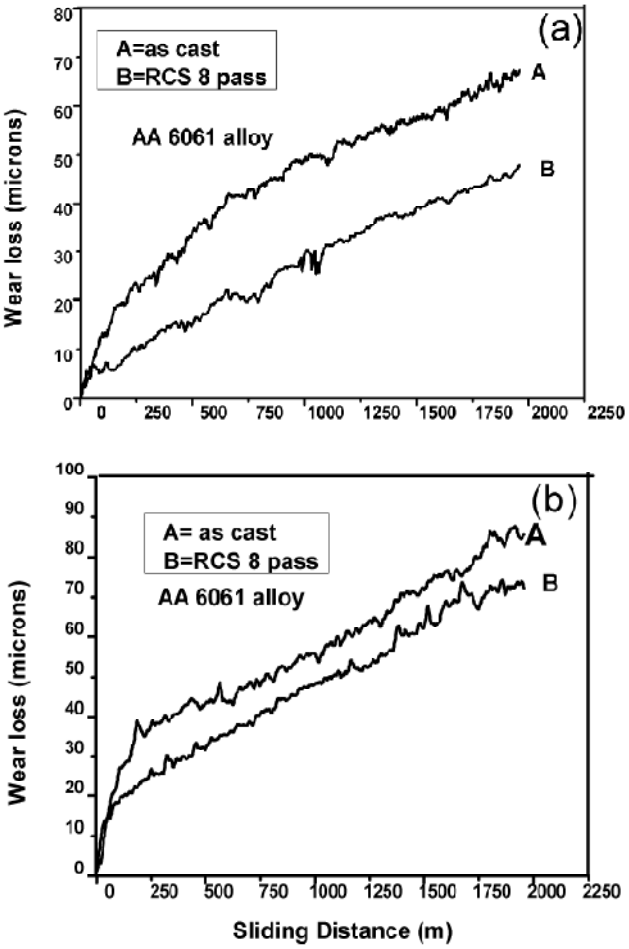

Fig. 3: Wear loss versus sliding distance for as cast and 8 pass RCS samples at (a) 5N and (b) 10N

typically of mild wear nature and at later sliding distances; the wear phenomena is of severe sliding wear phenomena. This type observation is observed in both cases for the samples in as cast condition and RCS processed conditions. As expected, the wear loss observed for 10 N applied was more as compared to the samples of as cast and RCS processed for 5N applied load.

Scanning electron microscopy studies

The SEM images of as cast and RCS processed 6061 alloy subjected to 5N and 10N loads tested at 2 m/s and sliding distance of 2000 m are shown in Fig.3 a, b. It can be seen from the images that a continuous deep ploughing grooves on the wear surface, and abrasion phenomenon is seen at 5N and 10 N loads in as cast and RCS processed samples.

The wear loss of the as-cast AA6061 alloy was higher than that of the RCS processed sample at all applied loads. These results clearly depicts that the wear resistance of RCS processed samples are higher than the as cast samples, as there was a drastic reduction in grain size due to severe

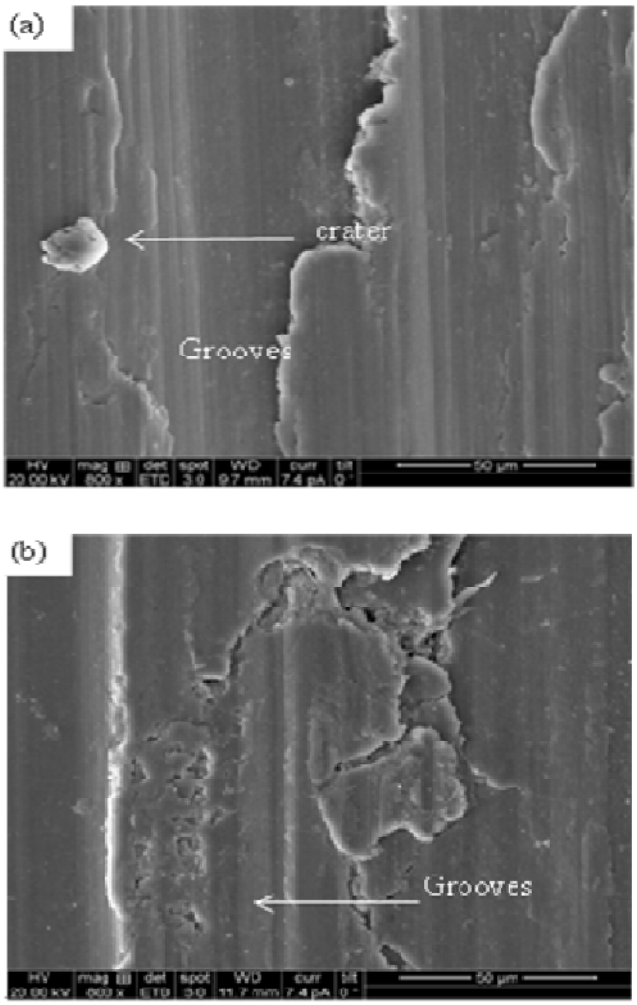

Fig. 4: SEM images of worn surfaces of (a) As-cast AA6061 alloy, Load=5N Sliding distance=2000 m (b) As-cast AA6061 alloy Load=10 N Sliding distance=2000 m

strain induced due to RCS process. The wear loss was found to decrease with increasing applied load for samples, indicating an improvement in wear resistance, especially at higher applied load. According to Yasmin et al. and Kori et al. **[20, 21]** sliding at higher applied load increases the strain hardening of the materials that are in contact. The increase in load leads to more frictional force that causes larger deformation and delaminated crater from the surface of the materials due to dislocation motion, so the material reveals the strain hardening in the sample. A s a result, the resistance to abrasion increases resulting in an increased wear resistance.

Figure 5 shows the SEM images of worn surfaces of RCS processed samples under applied load of 5 N and 10 N. The worn surface details clearly depict damage like microgrooves and craters. The presence of craters in the worn surface is due to the detachment of wear debris during the delamination wear **[22]**. It was observed that the craters and grooves were found in the as cast AA6061 alloy while

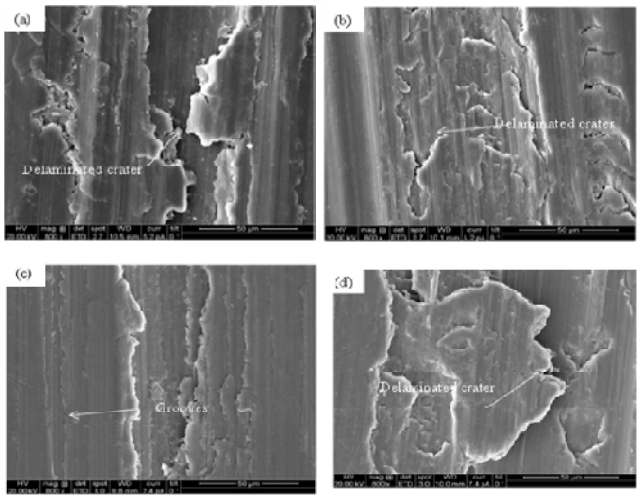

Fig. 5: SEM micrographs of wear surfaces (a) RCS 8 pass wor. of AA6061 alloy Load=5N Sliding distance=2000 m (b) RCS 8 pass wor AA6061 alloy Load=10 N Sliding distance=2000 m (c) RCS 8 pass wr of AA6061 alloy Load=5N Sliding distance=2000 m (d) RCS 8 pass wr AA6061 alloy Load=10 N Sliding distance=2000 m

the main surface damage on the RCS processed sample was grooves and abrasive scoring marks indicates that delamination wear took place. This prevails that the less delamination wear in case of RCS as compared to as cast for various parameters viz., applied loads, sliding distance and rpm of steel disk. It indicates improvement in the wear resistance property could be due to the higher hardness of RCS sample than as cast AA 6061 alloy. An increase in hardness leads to reduction in the adhesion and delamination of the sample, in turn decreasing the wear rate in RCS sample. It can be concluded that RCS sample got reduction in grain size that could lead to increase in higher hardness to as cast AA 6061 alloy that improves the wear resistance property in the RCS sample.

4. CONCLUSIONS

- AA6061 samples were successfully processed up to 8 passes using RCS design.
- The RCS processed AA 6061 sample exhibited hardness of 120 VHN. This is due to the reduction in grain size of the sample due to intensive strain induced due to RCS processing.
- The higher hardness of RCS processed sample exhibited higher sliding wear resistance as compared to a cast 6061 alloy.
- Worn surface microstructural details suggest high wear loss in the AA 6061 alloy in as cast samples is due to micro deep ploughing grooves and craters.
- The worn surface and its microstructural details of RCS processed sample after eight passes without rotation

and with rotation suggest in delamination wear and crater because of higher hardness.

ACKNOWLEDGEMENTS

Our sincere thanks to **Principal Dr Ashok S. Shettar** K.L.E.Society B.V.B.College of Engg. and Technology Hubli Karnataka for his support & encouragement and **Dr S.A. Kori Basaveshwar Engineering College Bagalkot Karnataka**, he helped us to make use of RCS facility for processing.

REFERENCES

1. Terry B. and Jones G., In Metal Matrix Composites-Elsevier Advanced Technology, 1990.
2. Charles D., Metal Matrix Composites,Met.Mater.,6 (1990) 78.
3. Zedalis M.S., Bryant J. D., Gilman P.S. and Das S.K.,Jour. Met.43(1991) 29.
4. R.Z. Valiey, R.K. Islamgaliev, I.V. Alexandroy, Prog. Mater. Sci. 45 (2000) 103.
5. Sahin. Mater. Des. 28 (2007). 1348.
6. K. Venkateswarlu,, V. Rajanikanth, A.K. Ray,C.Xu, T.G. Longdon, Mater. Sci. Eng. A 527 (2010) 1448.
7. K. Venkateswarlu, V. Rajinikanth, A.K. Ray, C. Xu, T.G. Langdon, Rev. Adv. Mater.Sci. 25 (2010) 99.
8. K.Venkateswarlu, V. Rajinikanth, M.K. Sen, S.N. Alhajeri, T.G. Langdon, Mater. Sci. Forum 667(2011) 743.
9. R.Z. Valiev, T.G. Langdon, Prog. Mater. Sci. 51 (2006) 881.
10. A.P. Zhilyaev, T.G. Langdon, Prog. Mater. Sci. 53 (2008) 893.
11. Kalaiselvan K., Murugan N., Parameshwaran S., Mater. Des. 32 (2011), 4004.
12. S. Basavarajappa, G. Chandramohan, Arjun Mahadevan, Mukundan Tangavelu, R. Subramanian, Wear, 262 (2007), 1007.
13. Sarkar K,Clarke H. Material Science 194,(1988),1785.
14. Jiang J., Stott F.H., Stack M.M. Wear,183,(1995),20.
15. Dutta,I., Allan S.M., Hafley J.L. Journal of Meta. And Mater. Trans. A 22(1991) 2553.
16. Mitra R., Rama Rao V.V., Mahajan Y.R. Mater. Sci. and Tech. 13 (1997) 415.
17. S.C. Pandey, M.A. Joseph, M.S. Pradeep, K. Ragahavendra, V.R. Ranganath, K. Venkateswarlu, T.G. Longdon, Mate Sci. Eng. A-Struct, 534 (2012) 282.
18. V. Rajinikanth, G. Arora, N. Narasaiah, K.Venkateswarlu, Mater. Lett. 62 (2008) 301.
19. Y. Estrin, A.Vinogradov, Acta Materialia 61 (2013) 782.
20. Yasmin T. Khalid AA, Haque M., Journal mater. process technology 153 (2004) 833.
21. Kori S., Chandrashekharaiah T., Wear 263 (2007) 745.
22. Abd EI Aal MI, EI Mahallawy N, Shehata FA, Hameed m, Yoon EY, Kim H S., Mater. Sci. Eng. A 527 (2010) 3726.

FRICTION AND WEAR BEHAVIOUR OF HOT FORGED AL6061-TIC IN-SITU MMC'S

G.S. Pradeep Kumar[1*] and R. Keshavamurthy [2]

[1]Assistant Professor, Automobile Engineering, Dayananda Sagar College of Engineering, Bangalore - 560078, India.
[2] Professor, Mechanical Engineering, Dayananda Sagar College of Engineering, Bangalore - 560078, India.
* Corresponding Author's mail id - pradeepgs.87@gmail.com

KEY WORDS: ' In-situ composite, Al6061, TiC, Forging, Friction, wear'

ABSTRACT

Al6061-TiC metal matrix composite was fabricated by liquid metallurgy route via in-situ reaction, using the mixture of Al6061 alloy, Potassium hexaflourotitanate salt (K_2TiF_6) and graphite powder. The developed composites were subjected to open die hot forging. SEM studies, X-ray diffraction studies (XRD), microhardness and dry friction and wear tests were carried on the cast and forged composites. Pin on disc machine was employed to perform friction and wear tests. SEM and XRD studies confirms formation of fine in-situ TiC particles. Composites exhibited higher microhardness, improved wear resistance and lo wear coefficient of friction when compared with unreinforced alloy under identical test conditions. Further, performance of forged alloy and its composites were superior compared to its cast counter parts.

INTRODUCTION

Aluminium based metal matrix composites have been one of the key research areas in materials processing field in the last few decades. Recently, researchers are focusing on developing easily affordable, high quality metal matrix composites. In-situ method of processing metal matrix composites one such technique involves synthesis of reinforcing particles within the matrix material and offers several desirable properties over ex-situ or conventional techniques. Advantages of in-situ composites include, fine and uniform distribution of reinforced particles with good interfacial bond between matrix and reinforcement **[1-6].**

Birol**[7]** has reported on In situ formation of TiC particles in the Al/K_2TiF_6/graphite system: Al_3Ti forms as soon as the K_2TiF_6 and graphite mixture is added to the melt. Some reaction between the Ti released from the halide salt is taking place initially before Al_3Ti starts precipitating out. However, the fraction of TiC thus formed is rather small Al_3Ti particles dissolve in the melt with increasing temperatures and with time TiC. And has concluded that the number and size of Al_3Ti particles gradually decrease while TiC particles are noted in increasing numbers during isothermal holding at 1000°C. After 30 min at 1000°C yields a composite sample with pre-dominantly TiC particles is obtained. Tyagi **[8]** etal have studied dry sliding wear behavior of Al-TiC metal matrix composite. He has reported that wear rate of the composite found to be following archards law linearly with load. The wear rate was lower in composites when compared to base material. Has has observed oxidative wear mechanism in the composite for a given test conditions. Jayasheel etal **[9]** have reported that addition of TiC particles in Al2219 matrix alloy by stir casting process improved the wear resistance of the composite. Further, wear resistance of the composite enhanced with increased content of TiC. Rajnesh tyagi**[10]** Have studied that TiC wear rate increases linearly with increasing normal load and also concluded that wear rate also decreases linearly with increasing volume fraction of titanium carbide and average coefficient of friction decreases with increasing load in both pure aluminium and composites and the composites show a lower coefficient of friction than pure al uminium. Chaitanya etal **[11]** have studied microstructure and hardness of Aluminum-TiC Composite fabricated by using stir casting route via halide salt reaction method. They have observed that TiC particles are distributed throughout the matrix and composite exhibited a noticeable improvement in hardness. However, from the extensive literature review, it is noticed that very meager informataion is available as regards hot forged Al based MMC's.

In the light of the above present investigation deals with Tribological characterization of cast and forged In-situ Al6061-TiC composites processed by liquid metallurgy route.

EXPERIMENTAL DETAILS

Al6061-TiC composites were prepared by first melting the base Aluminium 6061, obtained in a graphite crucible using electric resistance furnace. Molten Aluminium alloy maintained at a temperature of 900°C was added with Potassium hexafluorotitanate salt (K_2TiF_6) (600) grams and a graphite powder (40grams) in a stoichiometric ratio to obtain, 5wt%, 10wt% TiC. The molten composite mixtures were stirred constantly by a mechanical stirrer for its uniform distribution of TiC throughout the base metal. The cast metal matrix composites and Aluminium 6061 alloy were subjected

Table-1 : Chemical composition of Al6061 alloy

Elements	Si	Fe	Cu	Mn	Ni	Pb	Zn	Ti	Sn	Mg	Cr	Al
Percentage	0.43	0.43	0.24	0.139	<0.05	0.024	0.006	0.022	0.001	0.802	0.184	Balance

to open die hot forging at a temperature of 500°C at a constant strain rate. More details on the composite preparation and forging are available in our earlier works [2]. Both cast and forged Al6061 alloy and Al6061-TiC composites were subjected to SEM studies, XRD, microhardness test and friction and wear test. SEM studies were carried out by using JSM 840a Jeol scanning electron microscope at Indian Institute of Science, Bangalore, India. Microhardness tests were conducted using Vickers microhardness tester at a load of 100 grams for duration of 10 seconds. An average of five indentations were taken has hardness of each sample. Friction and wear studies were carried out as per ASTM G99 standard test method using Pin on disc type machine, (Model: TR20 Tribometer, Make: Ducom Instruments Pvt.Ltd. Bangalore, India). Machined samples of size 8mmF and 20mm length were used as test specimens. Counterface disc was made of EN-31 steel and hardened to 60HRC. A track radius of 30mm and test duration of 30 minutes was adopted for all the tests. The loads and sliding velocities were in the range of 20N to 100N and 0.314m/s to 1.574m/s respectively. Frictional force was recorded using load cell of 0.1N accuracy and wear loss was measured using linear variable differential transducer (LVDT) of accuracy 1µm. The coefficient of friction was calculated using frictional load and normal load data. The wear rates were calculated from height loss data in terms of volumetric wear loss per unit sliding distance.

RESULTS AND DISCUSSIONS

Scanning Electron Microscopy

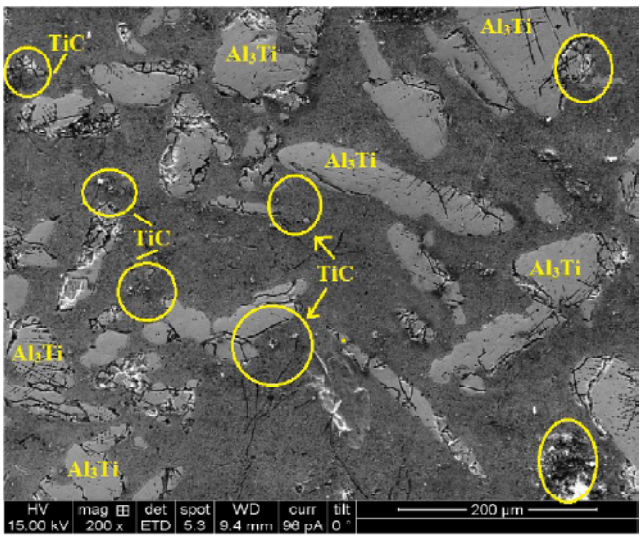

Fig. 1: Cast Al6061-10wt%TiC composite

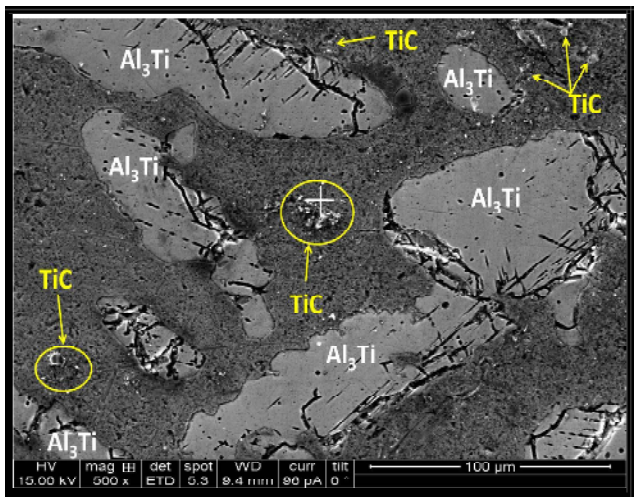

Fig. 2: Hot Forged Al6061-10wt% TiC composite

X-RAY Diffraction Analysis

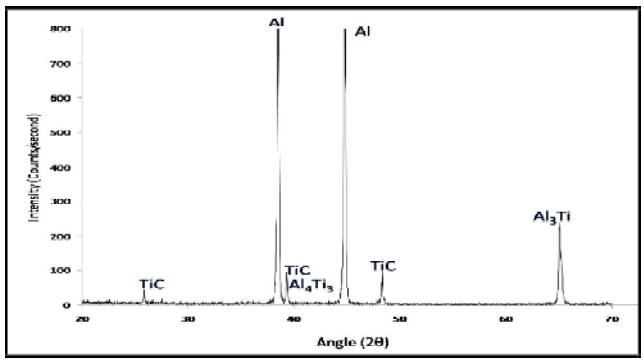

Fig. 3: X-ray difraction pattern of Al6061-10wt%TiC composite

Fig. (1-2) shows scanning electron micrographs of Al6061-10wt%TiC and in-situ metal matrix composite under cast and forged conditions. It is observed that fine particles of size in 2-10 mm are distributed in an uniform manner throughout the matrix alloy in both cast and forged conditions. Further, the micrograph also shows other dominant phases such as Al_3 Ti, Al_4C_3 Brittle phases In addition to in-situ formed TiC particles. Fig. 3 reports X-ray diffraction pattern of Al6061-TiC Composite. X-ray diffraction pattern of Al6061-TiC Composite reconfirms presence of TiC particles in the developed composite in addition to Al_3Ti and Al_4C_3 phases.

Microharness

Fig.4 shows variation of microhardness of as cast and hot forged Al6061 alloy and Al6061-TiC In-situ metal matrix

composite. It is observed that composite shows a higher microhardness when compared with matrix alloy in both as cast and hot forged conditions. Further, microhardness increases with increase in the percentage of TiC particles in both as cast and hot forged conditions. This may be due to fact that the large difference in coefficient of thermal expansion between TiC and matrix alloy results in higher density of dislocations leading to higher hardness. Extensive grain refinement after hot forging will act as obstacles for dislocation motion and enhances the hardness. [2,6].

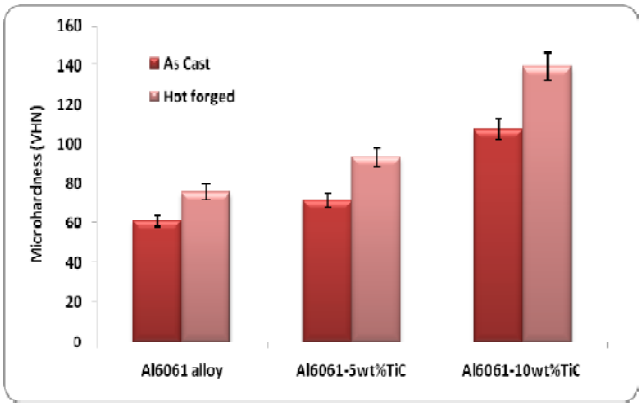

Fig. 4: Variation of microhardness in Al6061- TiC composite

Friction and Wear

Coefficient of Friction (COF):

Fig. 5 shows the variation of coefficient of friction of Al6061 alloy and Al6061-TiC composite. It is observed that coefficient of friction of composites reduces with formation of TiC particles. For a given load and sliding velocity, a maximum of 9% decrease in coefficient of friction is observed in the developed in-situ composite when compared with unreinforced alloy. The lower value of coefficient of friction of composite may be attributed to antifrictional properties of In-situ formed TiC particles. The decrease in coefficient of friction may be attributed to fact that during sliding process the presence of in-situ TiC particles results in formation of oxides of iron and aluminum which will shear in the interface

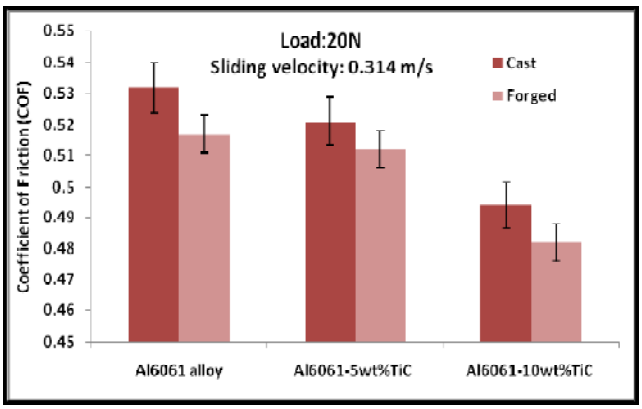

Fig. 5: Variation of COF of as cast and forged Al6061 alloy and Al6061-TiC composite

leading to lower coefficient of friction **[3]**. Fig.6 and Fig.7 shows influence of load and sliding velocities on coefficient of friction of matrix alloy and developed composite respectively. It is clear from the graph that with increase in load a reduction in coefficient of friction is observed in both matrix alloy and in-situ composite. However, at all the loads studied, forged alloy and its composite exhibited reduced coefficient of friction when compared with cast matrix alloy and its composites. It is also observed that coefficient of friction increases with increase in sliding velocity.

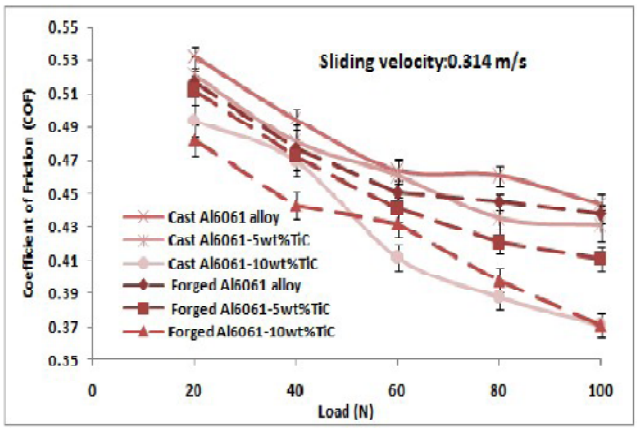

Fig. 6: Variation of COF of as cast and forged

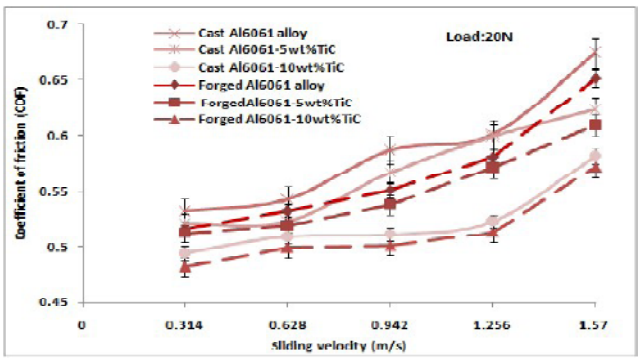

Fig. 7: Variation of COF of as cast and forged alloy and composite with load alloy and composite with sliding velocity

Wear Rate

Fig. 8 shows the effect of in-situ TiC formation on wear rate of Al6061 alloy. Under identical test conditions the wear rate of in-situ composite is significantly lower than unreinforced ones. For a given load and sliding velocity, a maximum of 39% decrease in wear rate is observed in the in-situ composite when compared with matrix alloy. Improved wear resistance may be attributed to higher hardness and load bearing capacity of composite. Fig. 9 and Fig. 10 shows influence of load and sliding velocities on wear rate of matrix alloy and in-situ composite respectively. It is observed that with increase in load, an increase in the wear rate is noticed in both matrix alloy and In-situ composite. Increased wear rates with increased load can be attributed to large plastic deformations which promote the larger extent of wear debris formation leading to higher wear rates **[3, 9-10]**. Fig.10

shows the dependence of wear rates of Al 6061 matrix alloy and In-situ composite on sliding velocity. With an increase in sliding velocity there is an increase in wear rate for both matrix alloy and composite. However, at all the sliding velocities studied, the wear rate of the composite was much lower when compared with the matrix alloy. Further, under all the test conditions studied, wear rate of forged alloy and its composites were considerably lower than their cast counter parts, which may be attributed to higher hardness, extensive grain refinement and homogeneity in distribution of reinforced phase as discussed earlier.

CONCLUSION

Al6061-TiC composite synthesized by in-situ reaction technique shows fairly uniform dispersion of TiC particles throughout the base alloy. Hot forged in-situ Al6061-TiC composites shows higher hardness and reduced co-efficient of friction and lower wear rates at all the loads and sliding velocities when compared with cast Al6061 alloy and Al6061-TiC in-situ composites.

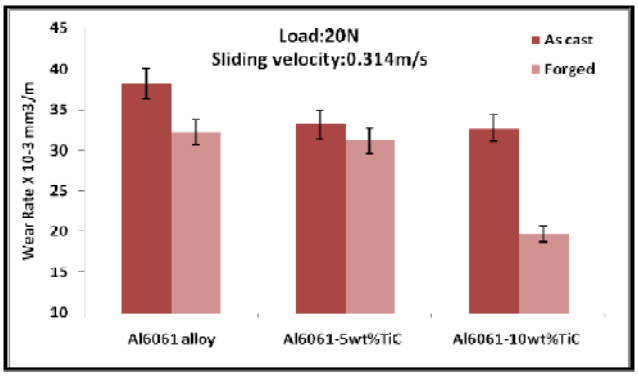

Fig. 8: Variation of wear rate of as cast and forged Al6061 alloy and Al6061-TiC composite

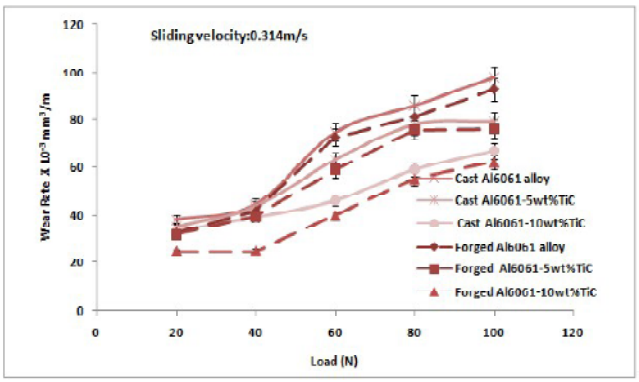

Fig. 9: Variation of wear rate of as cast and forged alloy and composite with load

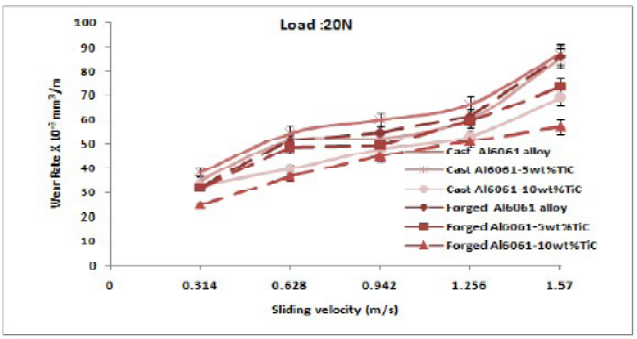

Fig. 10: Variation of wear rate of as cast and forged alloy and composite with sliding velocity

REFERENCES

1. Min. Zhao, Gaohui. Wu, Longtao. Jiang, Zuoyong. Dou, Friction and wear properties of Ti B_2 P / Al composite, Composite Part A: Applied Science and Manufacturing. **37** (2006) 1916–1921.
2. G.S. Pradeep kumar, R.Keshavamurthy, C.S. Ramesh, T.P. Bharatesh Mechanical properties of Hot forged Al6061-TiB_2 In-situ Metal Matrix composites Materials today proceedings volume 2, Issues 4-5, pp. 3107-3115.
3. G.S. Pradeep kumar, R. Keshavamurthy, C.S. Ramesh, B.H.Channabasappa Tribological characteristics of Al 6061-TiC composite synthesized by In-situ Technique: Applied mechanics and materials Vol. **787**(2015), pp 653-657.
4. S. Kumar, M. Chakraborty, V. Subramanya Sarma, B.S. Murty, Tensile and wear behaviour of In- situ Al–7Si/TiB_2 particulate composites, Wear. **265** (2008) pp.134–142.
5. Gao, Q., Wu, S., Lü, S., Duan, X. & Zhong, Z. (2015). Preparation of in-situ TiB_2 and Mg_2Si hybrid particulates reinforced Al-matrix composites. *Journal of Alloys and Compounds*, 651, pp. 521-527.
6. R. Keshavamurthy, S. Suhael Ahmed, A. Mudashi Laxman, N.H. Anil Kumar, M.N. Shashidhara, Y. Vimarshan Reddy, Tribological properties of Hot forged Al2024-TiB_2in-situ composite, Advanced Materials Manufacturing & Characterization Vol. 4, Issue **2** (2014), pp-87-92.
7. Y. Birol. "In situ synthesis of Al–TiC composites by reacting K2TiF6 and particulate graphite in molten aluminium". Journal of Alloys and Compounds **454** (2008), pp 110–117.
8. Rajnesh Tyagi "Effect of TiC Content on Friction and Wear Behavior of Al-TiC Composites", pp. 9-10; 2 pages, World Tribology Congress III, Volume 1.
9. Jayasheel I. Harti, B. R. Sridhar, H. R. Vitala, Pankaj R. Jadhav, Wear Behavior of Al2219-TiC Particulate Metal Matrix Composites, American Journal of Materials Science p-ISSN: 2162-9382 e-ISSN: 2162-8424, 2015; **5**(3C): pp 34-37.
10. Raj Nesh Tyagi, "synthesis and tribological characterization of in situ cast Al-TiC composites" wear **259**(2005), pp 569-576.
11. D. Sai Chaitanya Kishore, Dr K. Prahlada Rao, Dr. A. Mahamani "Fabrication and characterisation of In-situ Al-TiC Composite" ISSN Volume 4 Jan-feb (2013), pp. 109-114.

PERFORMANCE ANALYSIS OF CONICAL FLUID FILM HYDRODYNAMIC JOURNAL BEARING FOR VARIOUS ASPECT RATIO

Vikas M. Phalle[1], Ajay Kumar Gangrade[2*] and S.S. Mantha[3]

[1]Associate Professor, Department of Mechanical Engineering, VJTI, Mumbai 400 019, India
[2]Research Scholar (VJTI) and Faculty, K.J. Somaiya College of Engineering, Mumbai 400 077, India
[3]Professor, Department of Mechanical Engineering, VJTI, Mumbai 400 019, India
*Corresponding author (E-mail: akgangrade@somaiya.edu)

KEY WORDS: Hydrodynamic journal bearing; CFD; Aspect ratio; Semi cone angle; Lubrication

ABSTRACT

High speed and high power rotating machines, i.e. turbine, compressor etc. is commonly supported on fluid film bearings and demand for continuous improvement in application. Conical fluid film hydrodynamic journal bearing, having ability to support the load in radial as well as in axial direction has been presented as a modification for plain circular hydrodynamic journal bearing. In the present research work, the effectsof semi cone angle (10°, 20°and 30°) and aspect ratio (0.5, 0.8, and 1.0) on the pressure distribution of conical fluid film hydrodynamic journal bearings have been studied for Newtonian fluid (oil, water and glycerin) using Computational Fluid Dynamic (CFD) software package. The maximum pressure at the mid plane of conical hydrodynamic journal bearing is significantly improved with increase insemi cone angle and aspect ratio. The objective of this research work is to report the various configuration of conical hydrodynamic journal bearings as an option to replace two separate bearings i.e. journal and thrust bearing in precision machines.

INTRODUCTION

The hydrodynamic journal bearings have considerable benefits and widely used in industry because of their simplicity, efficiency and low cost. The oil film also provides shock absorbing capability and damping as a design parameter to control vibrations in the rotating machines. These benefits promoted the hydrodynamic journal bearing to be used in industry for high load and high speed applications. Conical fluid film hydrodynamic journal bearings have significant advantages over cylindrical journal bearings, such as an ability to support loads in the axial as well as in the radial direction and clearance is also easily adjustable on assembly. Sharma et al. **[1, 2]** have presented static and dynamic performance analysis of hydrostatic/ hybrid conical journal bearing with the influence of wear. They have solved Reynolds equation using FEM and the Newton Raphson method and suggested that the increase in the value of a semi cone angle increases the axial load carrying capacity of the bearing. The results of this study encouraged the author to control the geometry of the bearing with aspect ratio and semi cone angle with a uniform clearance for hydrodynamic conical journal bearing.

Yoshimoto et al. **[3]** investigated water-lubricated hydrostatic conical bearings with spiral grooves for high speed spindles. Their study revealed that the complaint surface bearing has a larger load carrying capacity in a relatively large bearing clearance than the rigid surface bearing. Korneev **[4]** investigated and compared the load carrying capacity of conical hydrodynamic journal bearings by Finite Difference Methods (FDM) for the rotors of various high speed turbines. The bearing parameters considered for this study were cone angle (15°, 30° and 45°) and eccentricity ratio (å= 0.2, 0.4 and 0.6).Murthy **[5]** presented the analysis of conical type hydrodynamic crown bearings for self-adjusting the working clearance for trouble-free service and extended the work for different lobe configurations as a design guide. Sumikura et al. **[6,7]** developed the concept to use conical hydrodynamic journal bearings in medical science for axial blood pump. They have developed the enclosed-impeller type axial flow bloodpump that enables an enclosed-impeller to be levitated using hydrodynamicconical bearings. They have used the hydrodynamic conicalbearing with aspect ratio less than one and glycerol solution as the working fluid. Heshmat et al. and Han Qing et al.**[8, 9]** developedahydrodynamicjournal bearing for the MiTiHeart®. Several bearingconfigurations were designed based on the taper-land configuration and tests were performed with blood analog (glycerin/ water).Theirresults indicatedthat the load carrying capacity and power loss were dependentonbearing geometry, film thickness and fluid film properties.Ferron et al., Jagadeesha et al., Gertzos et al.and other investigators**[10-15]** worked in the area of fluid film hydrodynamicjournal bearing with different aspect ratio and operating conditions.

A thorough scan of the available open literature reveals that the most of the studies mainly focused on circular hydrodynamic and conical hydrostatic/hybrid journal bearing system**.** However, very few studies are available onhydrodynamic conical journal bearing. The present study is aimed to address this gap in literature and proposedthe

CFD investigation of a conical fluid film hydrodynamic journal bearing for various semi-cone angles and aspect ratio. This study also has been extended tovarious Newtonian fluids (oil, water and glycerin). The numerically simulated CFD results are expected to be quite useful to the bearing designer and the academic community.

ANALYSIS

A generalized form of Reynolds equation is derived from the fundamental equations of hydrodynamics and it will be reduced to use in the analysis of fluid-film bearings. The modified Reynolds equation governing the fluid flow in the clearance space of a conical journal and bearing in spherical coordinate is expressed as **[1]**

$$\frac{1}{r}\frac{\partial}{\partial r}\left(\frac{r}{12\mu}h^3\frac{\partial p}{\partial r}\right)+\frac{1}{\sin^2\gamma}\frac{\partial}{\partial \varphi}\left(\frac{h^3}{12\mu r^2}\frac{\partial p}{\partial \varphi}\right)=\frac{\omega_J}{2}\frac{\partial h}{\partial \varphi} \quad ...1$$

The journal rotating with an angular velocity ù and rigid bearing with steady state equilibrium condition is assumed with the pressure generated by the lubricant film in clearance space of bearing. Schematic view of a conical hydrodynamic journal bearing supported on fluid film in clearance space is shown in Fig. 1.

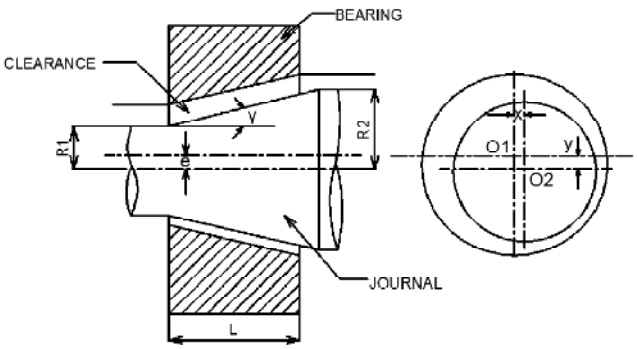

Fig. 1: Conical hydrodynamic journal bearing

In the present CFD analysis, 3-dimensional model Fig.2 has been prepared in GAMBIT by using dimensions and operating condition as referred in **[1, 10 and 11].** After Modeling of the conical journal bearing, the mesh file (.msh) created in gambit has been simulated in the ANSYS Fluent software for CFD analysis. Wodtke et al. **[16]** suggested that computer models are feasible alternative to experimental research for overcoming the cost and operational difficulty in experimental work.

The fluid flow in the clearance space of a journal bearing also has been discretized by using a four noded isoperimetric elements and the Lagrangian interpolation function, the pressure at a nodal point in the element is also solved with incorporating the boundary conditions and used to compare the CFD results. The overall solutions of conical hydrodynamic journal bearing have been found for unworn condition and Newtonian fluid as a lubricant with the following stages as per suggested by Sharma et al. **[1, 2].**

- Computation of fluid film pressure by solving Reynolds equations for the lubricant flow
- Examine of journal center equilibrium position
- Computation of static pressure in clearance space of bearing

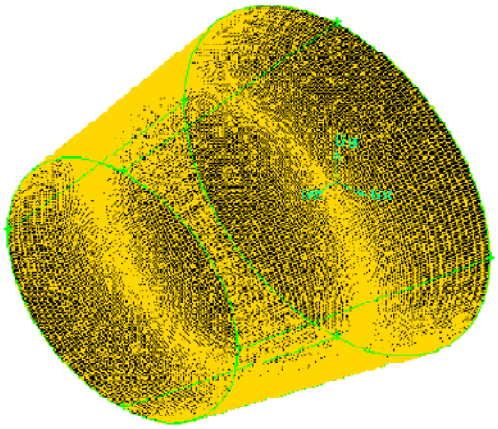

Fig. 2: Mesh of Conical hydrodynamic journal bearing

VALIDATION OF CFD RESULTS

The CFD results for non-dimensional maximum pressure values (p_{max}) at mid plane of the conical hydrodynamic journal bearing is validated by the code developed in Fortron-77 by using finite element method. Results show that maximum pressure ratio computed byCFD software were found in close range of 10% to 25%. The computed results for conical hydrodynamic journal bearing with semi cone angle ($\gamma = 20^O$) show a good agreement for various eccentricity ratios as shown in Fig. 3.

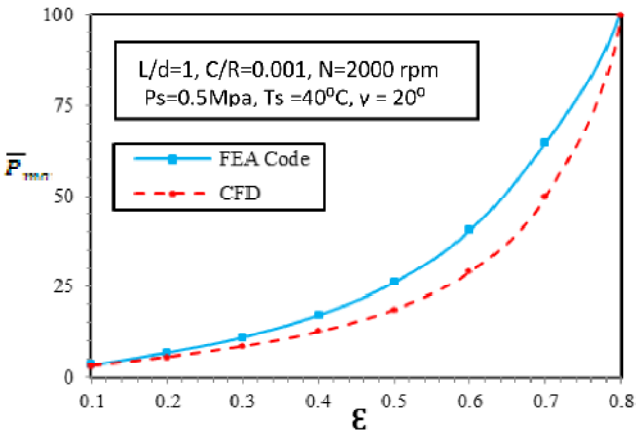

Fig. 3: Non Dimensional Pressure versus Eccentricity Ratio using FEA and CFD method

RESULTS AND DISCUSION

This study is carried out for the pressure distribution of conical fluid film hydrodynamic journal bearing for various aspect ratio (0.5, 0.8 and 1.0) and semi-cone angle ($\gamma = 5^o, 10^o, 20^o$ & 30^o). The study has been further

extended for different Newtonian fluids (oil, water and glycerin). The effects of aspect ratio and semi-cone angle on the pressure distribution of conical fluid film hydrodynamic journal bearing have been studied for various geometrical and operating parameters as mentioned in Table-1 and Table-2.

Table 1: Operating and geometric parameters for Conical hydrodynamic journal bearing

Geometric parameters	Notation	Values
Bearing aspect ratio	(λ)	0.5 , 0.8 , 1.0
Journal Mean Radius	R_{mean}	50 mm
Semi cone angle	(γ)	$5^o, 10^o, 20^o, 30^o$
Speed	(N)	2000 rpm
Eccentricity Ratio	([)	0.1 – 0.9
Clearance	(C)	50 micron
Supply Press. Gauge	P_s	0.5 Mpa
Operating Temp.	T_s	40°C

Table 2: Properties of fluids for CFD Analysis

Properties	water	Oil	Glycerin
Mass density (kg/m^3)	998.2	860	1259.9
fluid viscosity(*Pa-s*)	0.001003	0.0277	0.799
Specific heat (J/kg^OC)	4182	2000	2427
Thermal conductivity (w/m^OC)	0.6	0.13	0.286

CFD Analysis of bearing with various Aspect ratios

The analysis presented in this section uses model of conical hydrodynamic journal bearing in gambit software for various semi cone angles ($\gamma = 5^O, 10^O, 20^O, 30^O$) and aspect ratio ($\lambda = 0.5, 0.8, 1.0$). The comparative results for conical hydrodynamic journal bearing and cylindrical hydrodynamic journal bearing has been shown in Table-3 to evaluate the effect of semi cone angle on the performance of the bearing for eccentricity ratio ($\varepsilon = 0.6$). The selected pressure contour for semi cone angle ($\gamma = 10^O$) and various aspect ratio ($\lambda = 0.5, 0.8, 1.0$) of conical hydrodynamic journal bearings are as shown in Fig. 4 and Pressure v/s eccentricity ratio plot is also shown in Fig. 5.

Table 3: Pressure (in Pa) developed in conical and cylindrical bearing with various Aspect Ratios at ε = 0.6

Aspect ratio	Cylindrical JB ($\gamma = 0^O$)	Conical JB ($\gamma = 30^O$)	variation in P_{max} ($\gamma = 30^O$) v/s ($\gamma = 0^O$)
$\gamma = 0.5$	7.28×10^5	8.44×10^5	15.93%
$\gamma = 0.8$	9.17×10^5	1.13×10^5	23.23%
$\gamma = 1.0$	1.02×10^6	1.27×10^6	24.51%

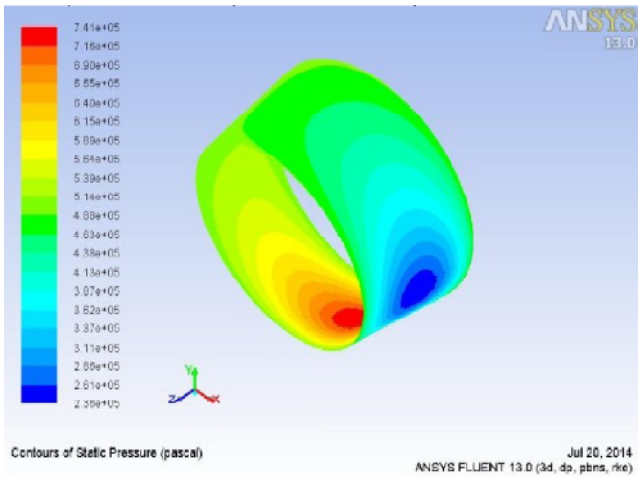

(a) Aspect ratio ($\lambda = 0.5$)

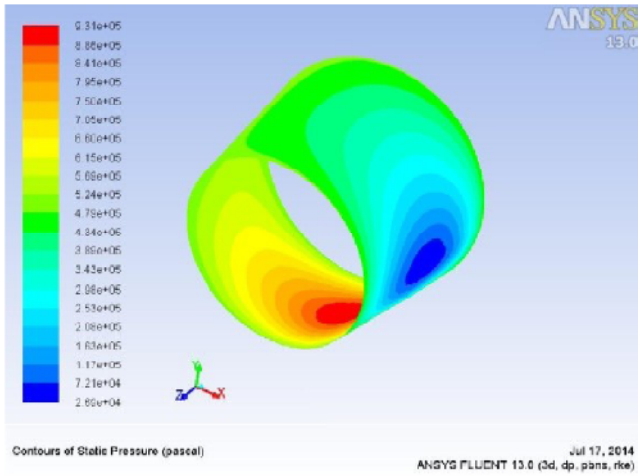

(b) Aspect ratio ($\lambda = 0.8$)

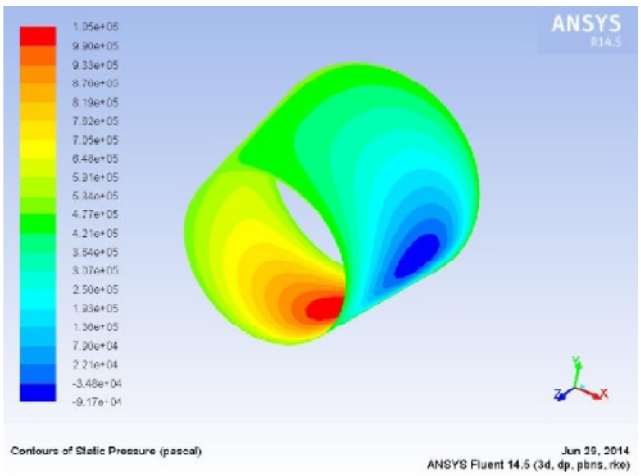

(c) Aspect ratio ($\lambda = 1.0$)

Fig. 4: Pressure contours for conical hydrodynamic journal bearings of semi cone angle ($\gamma = 10O$), eccentricity ratio ($\varepsilon = 0.6$), water as a lubricant for various aspect ratio ($\lambda = 0.5, 0.8$ and 1.0)

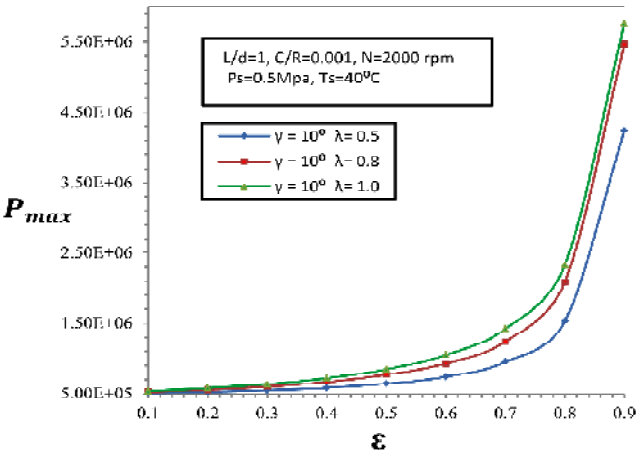

Fig. 5: Pressure v/s eccentricity ratio plot for conical hydrodynamic journal bearing with water as a lubricant semi cone angle ($\gamma = 10^{O}$), aspect ratio ($\lambda = 0.5, 0.8$ and 1.0).

CFD Analysis of bearing with various Lubricant fluids

The computational fluid dynamics model of conical hydrodynamic journal bearing with aspect ratio ($\lambda = 1.0$) has been simulated for various lubricants i.e. water, turbine oil and glycerin. The three configurations of conical hydrodynamic journal bearing of semi cone angle as 10^{O}, 20^{O} and 30^{O} have been considered for this analysis. Results of conical journal bearing ($\gamma = 30^{O}$) is comparedwith the plain cylindrical hydrodynamic journal bearingto see the effect of various lubricants on the performance of the conical bearingforeccentricity ratio ($\lambda = 0.6$) with aspect ratioas mentioned in Table 4.

Table 4: Pressure (in Pa) developed in conical and cylindrical bearing with various lubricating fluid

Lubricant Fluid	Cylindrical J B ($\gamma = 10^{o}$)	Conical J B ($\gamma = 30^{o}$)	Variation in p_{max} ($\gamma = 30^{o}$) v/s ($\gamma = 0^{o}$)
Water	1.02 x106	1.27 x106	24.51 %
Oil	12.31 x106	18.08 x106	46.87 %
Glycerin	3.35 x108	4.86 x108	45.07 %

Selected pressure contour for various lubricating fluid such as water, oil and glycerinfor conical hydrodynamic journal bearingsemi cone ($\gamma = 10^{O}$) and aspect ratio ($\lambda = 1.0$) with eccentricity ratio ($\varepsilon = 0.6$) are shown in Fig. 6. The percentage increase for p_{max} is more significant and prominent in case of lubricating fluid glycerin as compared to turbine oil and water liquid. Fig. 7 indicate that the maximum pressure is dependent on the eccentricity ratio and show the variation from 53.5% to 57.3% for the $\varepsilon = 0.2$ to 0.8.

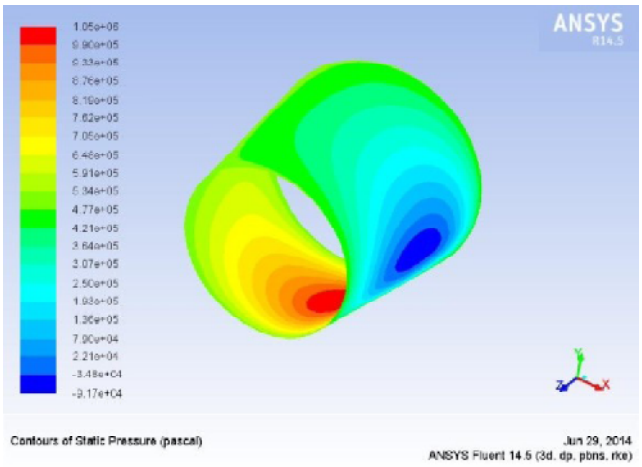

(a) Water as a lubricant

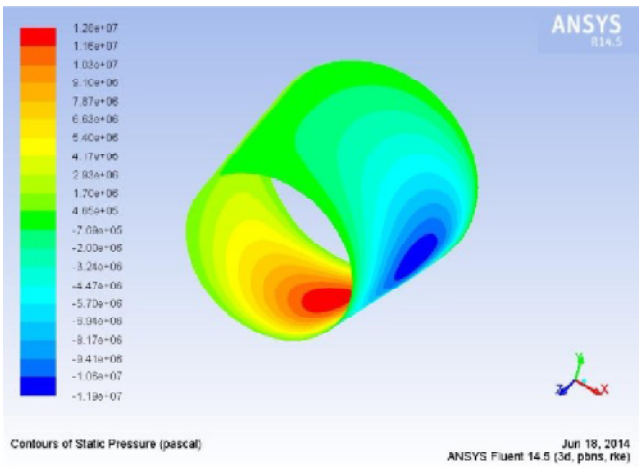

(b) Oil as a lubricant

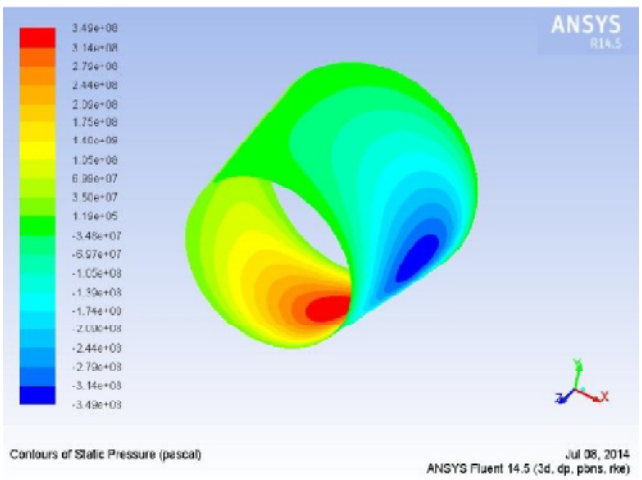

(c) Glycerin as a lubricant

Fig. 6 : Pressure contours for conical hydrodynamic journal bearings of semi cone angle ($\gamma = 10^{O}$), eccentricity ratio ($\varepsilon = 0.6$), aspect ratio ($\lambda = 1$) for lubricating fluid (Water, Oil, Glycerin) as a lubricant

Fig. 7 also shows the value of p_{max} for glycerin in the order of approximate 27 times corresponding to turbine oil lubricant. While the value of p_{max} for turbine oil in the order

of approximate 13 times corresponding to water liquid as a lubricant.

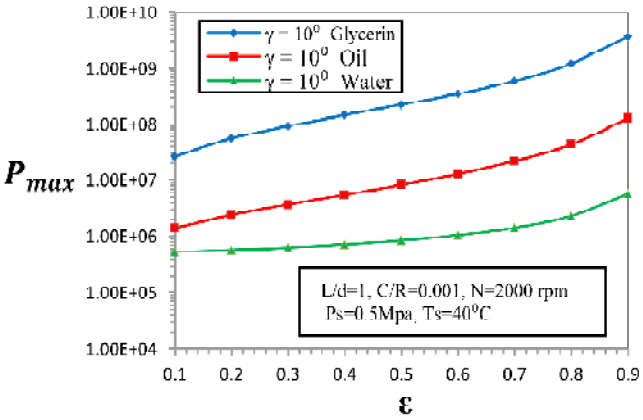

Fig. 7 : Pressure v/s eccentricity ratio plot for conical hydrodynamic journal bearings of semi cone angle (γ = 10°), aspect ratio (λ = 1) for various lubricating fluid (Water, Oil, Glycerin) as a lubricant

CFD Analysis of bearing for various semi cone angles

Pressure contours for conical hydrodynamic journal bearings of semi cone angle (γ = 10°, 20° & 30°), aspect ratio (λ = 1), eccentricity ratio (ε = 0.6) and water as a lubricant are shown in Fig. 8. While the plot of pressure verses eccentricity ratiofor semi cone angle (g = 10°, 20° & 30°), is shown in Fig. 9. Water lubricated bearing is commonly preferred in application such as ship building, transportation industry, food industry and pharmaceutical industry. Water lubricated bearing is having low load carrying capacity as compared to the turbine oil for all configuration of conical journal bearing (γ = 10°, 20°, 30°) hence to improve the load carrying capacity of water lubricated bearing higher aspect ratio is recommended.

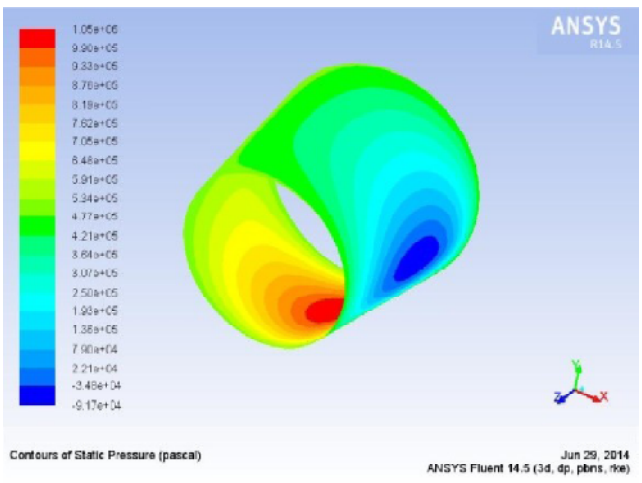

(a) Semi cone angle (γ = 10°)

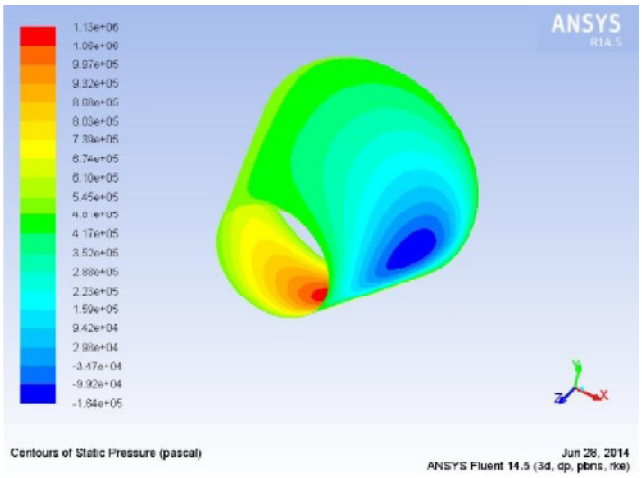

(b) Semi cone angle (γ = 20°)

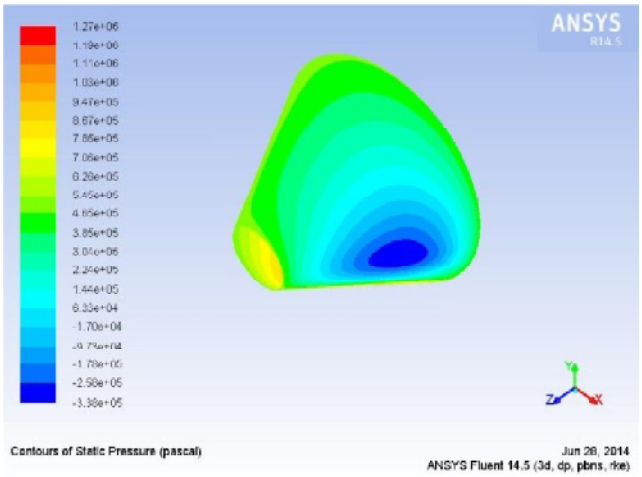

(c) Semi cone angle (γ = 30°)

Fig. 8 : Pressure contours for conical hydrodynamic journal bearings of aspect ratio (λ = 1), eccentricity ratio (ε = 0.6), water as a lubricant for various semi cone angle (γ = 10°, 20° & 30°)

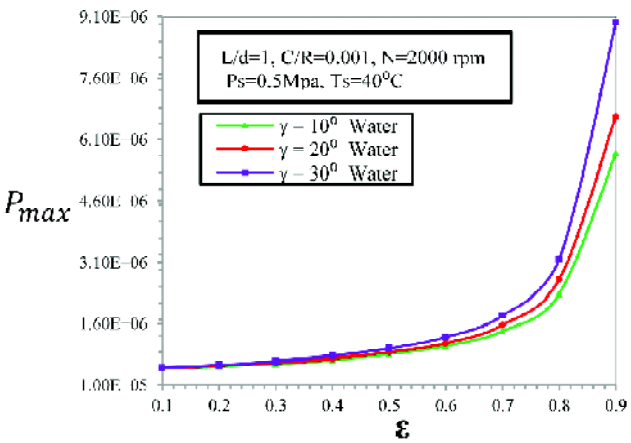

Fig. 9 : Pressure v/s eccentricity ratio plot for semi cone angle (γ = 10°, 20° & 30°), water as a lubricant and aspect ratio(λ = 1) for conical hydrodynamic journal bearing

CONCLUSIONS

The influence of aspect ratio (λ) and semi cone angles (γ) on the performance of conical hydrodynamic journal bearing has been studied for various Newtonian fluids (oil, water and glycerin) using CFD software package and FEA based program results. On the basis of numerically simulated results following conclusions may be drawn.

- × The maximum pressure at mid plane of conical hydrodynamic journal bearing significantly improved with increase in the value of an aspect ratio and semi cone angles along with eccentricity ratio.
- × A conical hydrodynamic journal bearing with semi cone angle $\gamma = 10^o$ shows a significant enhancement in the value of maximum pressure at mid plane of conical hydrodynamic journal bearing when glycerin is used as a lubricant as compared to oil and water liquid in present study.

Based on this analysis geometrical parameters such as aspect ratio (λ), semi cone angles (γ) and lubricating fluid for optimum performance of conical hydrodynamic journal bearing may be recommended for real bearing operating conditions.

ACKNOWLEDGEMENTS

The financial support from the All India Council for Technical Education (AICTE), New Delhi- India Ref. No. 8-221/RIFD/RPS/Policy-1/2014-15 for this work is gratefully acknowledged.

REFERENCES

1. Satish C. Sharma, Vikas M. Phalle and S. C. Jain, "Performance analysis of a multi - recess capillary compensated conical hydrostatic journal bearing system", Tribology International, 2011, Vol. **44**, pp. 617–626.
2. Satish C. Sharma, Vikas M. Phalle and S. C. Jain, "Influence of wear on the performance of a multirecess conical hybrid journal bearing compensated with orifice restrictor", Tribology International, 2011, Vol. **44**, pp. 1754–1764.
3. S. Yoshimoto, S. Oshima, S.Danbara and T. Shitara," Stability of Water-Lubricated, Hydrostatic, Conical Bearings with Spiral Grooves for High-Speed Spindles", Transactions of the ASME 2002, Vol. 124, pp. 398-405.
4. A. Yu. Korneev, "Static Characteristics of Conical Hydrodynamic Bearings Lubricated by Turbine Oil", Russian Engineering Research, 2012, Vol. **32,** No. 3, pp. 251–255.
5. T.S.R. Murthy, "Analysis of multi-scallop self-adjusting conical hydrodynamic bearings for high precision spindles" Tribology international June 1981, pp 147-150.
6. Sumikura Hirohito, Fukunaga Kazuyoshi, Funakubo Akio and Fukui Yasuhiro, "Development of an axial flow blood pump with hydrodynamic conical bearings", ASAIO Journal: 2005, Vol. 51 - Issue 2, pp 34A.
7. Sumikura Hirohito, Fukunaga Kazuyoshi, Funakubo Akio and Fukui, Yasuhiro, "Improvement and evaluation of an enclosed-impeller type axial flow blood pump with hydrodynamic conical bearings", ASAIO Journal: 2006, Vol. 52 - Issue 2, pp 32A.
8. Heshmat Hooshang, Hunsberger Andrew Z., Jahanmir Said, Walton James F. and Tomaszewski Michael J., "Prediction of hydrodynamic bearing performance for cardiac assist devices,"ASAIO Journal: 2006, Vol. 52 - Issue 2 - p 51A.
9. Han Qing, Ruan Xiaodong, Chen Wenyu and FuXin, "Numerical simulation and experimental research on passive hydrodynamic bearing in a blood pump", Chinese Journal of Mechanical Engineering, 2013, Vol. **26,** No. 5, pp 967-973.
10. Ferron J., Frene J., and Boncompain R., "A study of the thermohydrodynamic performance of a plain journal bearing comparison between theory and experiments", Transactions of the ASME, 1983. Vol. **105,** pp. 422-428.
11. K. M. Jagadeesha, T. Nagaraju ,Satish C. Sharma and S. C. Jain, "3D surface roughness effects on transient non-newtonian response of dynamically loaded journal bearings", Tribology Transactions, 2012, Vol. 55:1, pp. 32-42.
12. K.P. Gertzos, P.G. Nikolakopoulos and C.A. Papadopoulos, "CFD analysis of journal bearing hydrodynamic lubrication by bingham lubricant", Tribol. International, 2008, Vol. 41, pp 1190– 1204.
13. F. P. Brito, A. S. Miranda , J. C .P. Claro, J. C. Teixeira, L. Costa and M. Fillon, "The role of lubricant feeding conditions on the performance improvement and friction reduction of journal bearings",Tribol. International, 2014, Vol. 72, pp 65–82.
14. GuoHong, Lai Xinmin and Cen Shaoqi."Theoretical and experimental study on dynamic coefficients and stability for a hydrostatic/hydrodynamic conical bearing", Journal of Tribology Oct. 2009, Vol. 131 / 041701-7.
15. W. M. Hannon and M. J. Braun, "Numerical solution of a fully thermally coupled generalized universal reynolds equation (GURE) and its application part 1: conical bearings", Tribology Transactions, 2007, Vol. **50:** 540-557.
16. Wodtke M., Schubert A., Fillon M., Wasilczuk M., PajaCzkowskand P. Large, 'Hydrodynamic thrust bearing: Comparison of the calculations and measurements', ASME J Tribology, 2014, Vol. **228**(9), pp 974-83.

NOMENCLATURE

C	Radial clearance
R	Mean journal radius
C/R	Clearance ratio
D	Mean journal diameter
L	Bearing length
λ	Aspect ratio *(L/D)*
e	Eccentricity of journal center ($e^2 = X^2 + Y^2$)
ε	Eccentricity ratio *(e /C)*
γ	Semi cone angles
N	Rotational speed (rpm)
	Rotational speed (rad/sec)
p	hydrodynamic pressure
p_s	Lubricant supply pressure
p_{max}	Maximum pressure ratio (p_{max}/p_s)
c_p	Lubricant specific heat
k	Lubricant thermal conductivity
ϱ	Lubricant density
μ	Lubricant viscosity

Research Article

PERFORMANCE ANALYSIS OF POWER LAW LUBRICATED GEOMETRICALLY IMPERFECT FOUR LOBE MULTI-RECESSED HYBRID JOURNAL BEARINGS

Dharmendra Jain[1] and Satish C. Sharma[2]
[1]Research Scholar, [2]Professor
[2] Tribology Laboratory, MIED, Indian Institute of Technology, Roorkee, 247667, India.
[*]E-mail: dharma.auto@gmail.com, [2]E-mail: sshmefme@iitr.ernet.in

Keywords: Four-lobe bearing, Geometric imperfection, Power law lubricant

ABSTRACT

The present study deals with the combined influence of non-Newtonian lubricant and geometric irregularities (barrel and undulation type) of journal on the performance of four lobe multirecess hybrid journal bearing compensated with capillary restrictor. A power law model has been used to characterise the physical behaviour of non-Newtonian lubricant. The modified Reynolds equation has been solved using FEM. The computed results indicate that combined influence of barrel shape journal and non-Newtonian lubricant makes the bearing stiffer and consequently enhance the stability of the bearing system.

INTRODUCTION

The non-circular journal bearing system is used to overcome the disadvantage of circular journal bearing such as poor stability and self-excited vibration characteristics at higher speed. Multilobe bearings are often used to reduce bearing system sensitivity to oil film whirl. At light load application, the four-lobe multirecess hybrid journal bearing is found to be more stable. Four lobe bearing provides excellent characteristics such as a higher value of fluid film stiffness and threshold speed margin than a circular bearing. Many researchers have been carried out experimental as well as theoretical study on non-circular journal bearings to evaluate its performance characteristics **[1-5]**. Ghosh and Satish **[6,7]** theoretically determined the stability and rotordynamic coefficients taking the different value of offset factor (0.5, 75, 1, 1.25 and 1.5) for four lobe and three lobe bearings.

Generally the bearing analysis is made by on the assumption of journal surface is free from geometric irregularities. But in actual practice, the irregularities are present with the journal surface due to improper machining operations. These journal irregularities are barrel shape, bellmouth and undulation (surface waviness). In recent times, many researchers have included these irregularities in their theoretical and experimental analysis of fluid film journal bearing. Mokhtar et al. and Chennabasavan **[8-10]** analytically as well as experimentally determined the influence of the geometric irregularities (barrel, bellmouth and undulation) in hydrodynamic bearing. Rajput and Sharma **[11, 12]** investigated the influence of different recess shape, micropolar fluid and geometric irregularities of journal on the performance of circular hybrid journal bearing. Very recently, Jain and Sharma **[13]** determined the combined influence of geometric irregularities of journal and power law lubricant on the performance of two-lobe multirecess hybrid journal bearing. Many studies have been reported which shows the influence of non-Newtonian lubricant on the bearing performance by using power law model for circular/non-circular hydrodynamic/hydrostatic journal bearing. It has been observed that the non-Newtonian lubricant characterized by power law model have significant influence on bearing performance characteristic which are mentioned in literature **[13,14]**.

A thorough review of literature reveals that the bearing performance is significantly influenced by type of lubricant, journal bearing configuration and geometric irregularities of journal. Further, the study concerning the influence of geometric imperfection of journal on the performance of four lobe hybrid journal bearing operating with power lubricant has not been reported so far. Therefore, the present work is aimed to study the performance of geometrically imperfect four lobe bearing operating with power law lubricant.

ANALYSIS

The configuration of geometrically imperfect four lobe hybrid journal bearing system shown in Fig. 1.The modified Reynolds equation for flow of lubricant in the clearance space of the bearing in non- dimensional form expressed as follows **[13,14]**

$$\frac{\partial}{\partial\alpha}\left[\bar{h}^3\bar{F}_2\left(\partial\bar{P}/\partial\alpha\right)\right]+\frac{\partial}{\partial\beta}\left[\bar{h}^3\bar{F}_2\left(\partial\bar{P}/\partial\beta\right)\right]=\Omega\frac{\partial}{\partial\alpha}\left(1-\bar{F}_1/\bar{F}_0\right)\bar{h}+\frac{\partial\bar{h}}{\partial\bar{t}} \qquad (1)$$

$\bar{F}_0$, $\bar{F}_1$ and $\bar{F}_2$ are cross film viscosity functions and are given by following relations:

$$\bar{F}_0 = \int_0^1 \frac{d\bar{z}}{\bar{\mu}}, \bar{F}_1 = \int_0^1 \frac{\bar{z}d\bar{z}}{\bar{\mu}}, \qquad \bar{F}_2 = \int_0^1 \frac{\bar{z}}{\bar{\mu}}\left[\bar{z} - \bar{F}_1/\bar{F}_0\right]d\bar{z}$$

Fluid-film thickness

For geometrically imperfect four lobe hybrid journal bearing, the fluid film thickness is expressed as follows [11,13].

$$\bar{h} = \frac{1}{\delta} - \left[\bar{X}_j - \bar{X}_L{}^i\right]\cos\alpha - \left[\bar{Z}_j - \bar{Z}_L{}^i\right]\sin\alpha + \bar{h}_{ir} \qquad (2)$$

where $\bar{h}_{ir}$ is contribution of geometric errors to the film thickness ($\bar{h}$)

$\bar{h}_{ir} = -\bar{a}_1 \sin\left(\frac{\pi\beta}{2\lambda}\right)$ (For barrel shape)

$\bar{h}_{ir} = \bar{a}_3 \sin(n_1\alpha + \psi)$ (For undulation shape)

$\bar{X}_j$, $\bar{Z}_j$ and $\bar{X}_L{}^i$, $\bar{Z}_L{}^i$ are journal centre and lobe centre coordinates respectively and δ is offset factor. a_1, a_3, λ, ψ and n_1 are the amplitude of geometric irregularities, aspect ratio, phase angle and number of undulations respectively. α and β are circumferential and axial coordinate of bearing.

2.2. Shear strain power law

In this model shear stress varies as some power of the shear strain rate and is described as **[13,14]**

$$\bar{\tau} = \bar{m}\left(\bar{\dot{\gamma}}\right)^n \qquad (3)$$

where n is known as power law index and $\bar{m}$ is known as consistency index.

The value of shear strain rate ($\bar{\dot{\gamma}}$) acquired at every Gaussian point of the element is described as:

$$\bar{\dot{\gamma}} = \left[\left\{\frac{\bar{h}}{\bar{\mu}}\left(\bar{z} - \frac{\bar{F}_1}{\bar{F}_0}\right)\frac{\partial\bar{p}}{\partial\alpha} + \frac{\Omega}{\bar{\mu}\bar{h}\bar{F}_0}\right\}^2 + \left\{\frac{\bar{h}}{\bar{\mu}}\left(\bar{z} - \frac{\bar{F}_1}{\bar{F}_0}\right)\frac{\partial\bar{p}}{\partial\beta}\right\}^2\right]^{\frac{1}{2}} \qquad (4)$$

Apparent viscosity term is used in non-Newtonian fluid instead of viscosity which is the function of shear strain rate obtained as:

$$\bar{\mu}_a = \frac{\bar{\tau}}{\bar{\dot{\gamma}}} = f\left(\bar{\dot{\gamma}}\right)$$

Finite element formulation

The lubricant flow domain has been discretized using four-noded quadrilateral isoparametric elements **[12]**. The pressure is considered to be distributed linearly over an element and approximated as follows.

$\bar{P} = \sum_{j=1}^{4} N_j \bar{P}_j$; N_j = shape function of elements

Following the usual assembly procedure for the elements in the entire discretized flow field, the following global system equation is obtained:

$$\left[\bar{F}\right]\{\bar{p}\} = \{\bar{Q}\} + \Omega\{\bar{R}_H\} + \dot{\bar{X}}_J\{\bar{R}_X\} + \dot{\bar{Z}}_J\{R_z\} \qquad (5)$$

Where, $[\bar{F}]$ = Global Fluidity matrix

$\{\bar{p}\}$ = Global nodal pressure vector

$\{\bar{Q}\}$ = global nodal flow vector

$\{\bar{R}_H\}$ = global column vectors due to hydrodynamic terms

$\{\bar{R}_X\}$, $\{R_z\}$ = global right hand side vector due to journal centre velocities in x and z direction.

Boundary condition

The boundary conditions used for the lubricant flow field are given as:

(i) Nodes situated on the external boundary of the bearing have zero pressure; $\bar{P}|_{\beta=\pm1.0} = 0$

(ii) Nodes situated on the recess have equal pressure.

(iii) Flow of lubricant through the restrictor is equal to the bearing input flow.

(iv) At the trailing edge of the positive region, pressure gradient is zero $\bar{P} = \frac{\partial\bar{P}}{\partial\alpha} = 0.0$.

$\bar{P} = \frac{\partial\bar{P}}{\partial\alpha} = 0.0$ is implemented in algorithm by using successive over-relaxation method in Gauss Siedel iterative method.

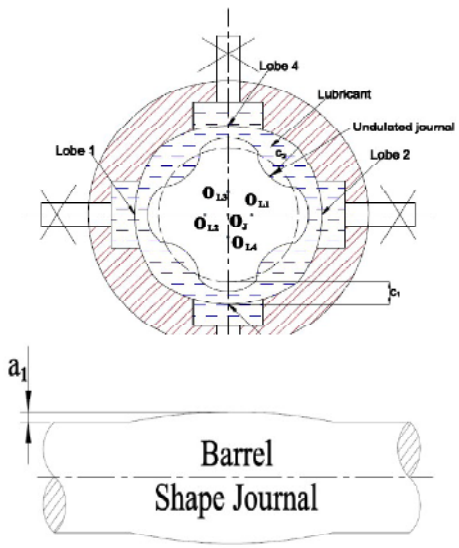

Fig. 1: Geometrically imperfect Four-lobe Hydrostatic/ Hybrid journal Bearing Configuration

RESULT AND DISCUSSION

The governing global system equation (4) has been solved using FEM incorporating usual boundary conditions. A computer program based on FORTRAN 77 has been developed to compute the performance parameters of four lobe bearing system. The geometric and operating parameters have been judiciously selected from the available literatures. Results of the present study have been validated with the previously published study [15] for power-law lubricant as shown in Fig. 2 .

The performance characteristics of four lobe bearing viz. fluid film thickness, direct stiffness/damping coefficients and marginal threshold speed with respect to external load have been computed and illustrated as follow.

FLUID FILM THICKNESS

Fig.2 shows that the bearing system with ideal journal provides higher value of $\bar{h}_{min}$ as compared to bearing with barrel and undulated journal .Circular journal bearing exhibit higher value of than four lobe bearing operating with Newtonian and non-Newtonian lubricant. The variation of film thickness is expected due the change in clearance space within the bearing systems. The order of increasing for different geometric irregularities (errors) shape journal is: barrel, undulation and ideal journal.

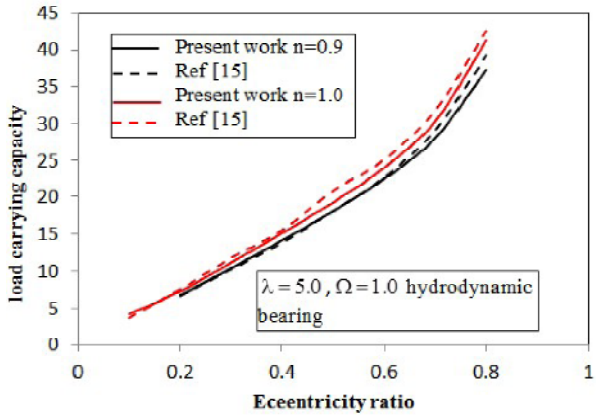

Fig. 2: Eccentricity ratio with load carrying capacity

Fluid film stiffness coefficient()

From Figs. (3), it may be observed that stiffness ($\bar{S}_{22}$) increases with increase in the value of load for both bearing configuration. Further, it also noted that the bearing operating with non-Newtonian lubricant possess higher value of fluid film stiffness ($\bar{S}_{22}$) than the bearing operating with Newtonian lubricant for both bearing configuration. The order of increasing stiffness ($\bar{S}_{22}$) for different geometric irregularities (errors) shaped journal is observed as: undulation, ideal journal and barrel shape for both bearing arrangement.

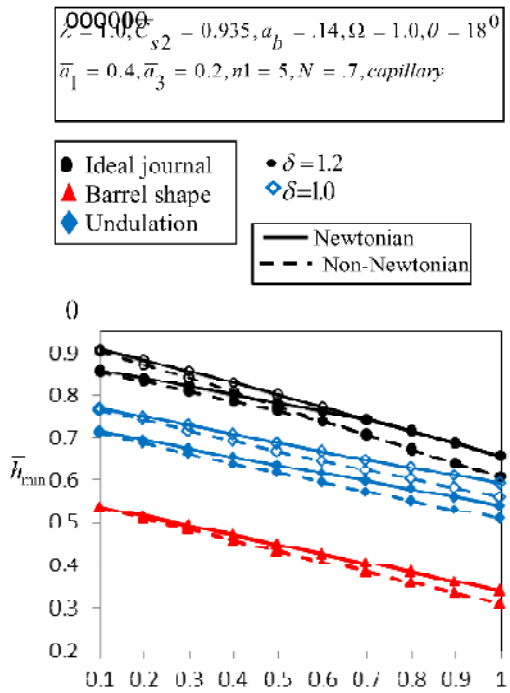

Fig. 3: Variation of $\bar{W}_0$ $\bar{h}_{min}$ with $\bar{W}_0$

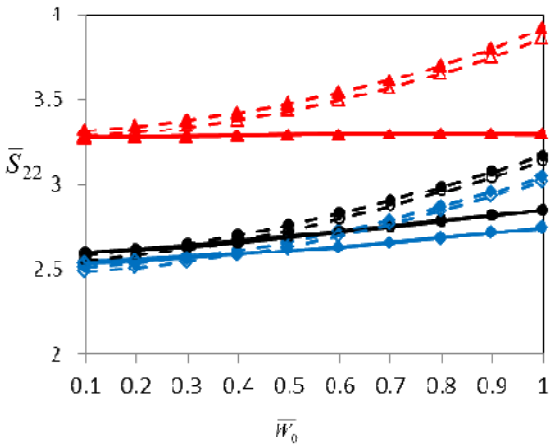

Fig. 4: Variation of $\bar{S}_{22}$ with $\bar{W}_0$

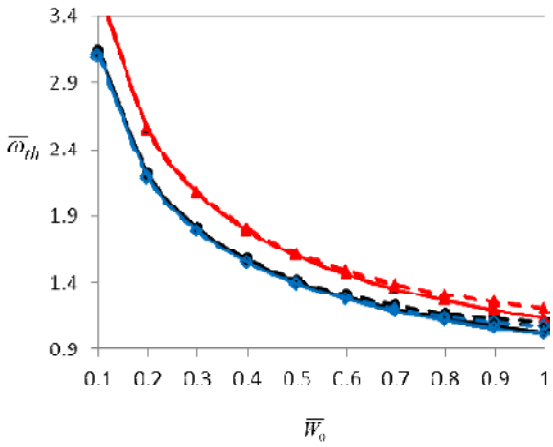

Fig. 5: Variation of $\bar{\omega}_{th}$ with $\bar{W}_0$

Stability threshold speed margin ($\overline{\omega}_{th}$)

From Fig.4, It may observed that four lobe bearing operating with Newtonian and non-Newtonian lubricant is more stable than that of circular journal bearing. Further, bearing with barrel shape journal is found to be more stable than with the rest of journal shapes. The order of increasing for bearing operating with Newtonian and non-Newtonian lubricant at different type of geometric irregularities (errors) shaped journal is as follows:

$$\overline{\omega}_{th}\big]_{\text{barrel shape}} > \overline{\omega}_{th}\big]_{\text{ideal journal}} > \overline{\omega}_{th}\big]_{\text{undulationl}}$$

CONCLUSION

The numerically simulated results reveal that geometric irregularities of journal, value of power law index and the value of offset factor significantly affect the bearing performance characteristics of four lobe hybrid journal bearing configuration. For higher values of external load, the bearing with barrel shape journal exhibits higher value of direct fluid film stiffness ($\overline{S}_{22}$) & stability threshold speed margin for power law lubricant vis-à-vis Newtonian lubricant.

REFERENCES

1. Pinkus, O., Lynn, W., and Mass. Analysis of elliptical bearing. ASME Trans, 1956, vol. **78**, pp.965–973.
2. Pinkus, O., Lynn, W., and Mass. Power loss in elliptical and 3-lobe bearings. ASME Trans., 1956, vol. **78**, pp. 899–904.
3. Lund, J.W. and Thomsen, K.K. A calculation method and data for the dynamic coefficients of oil-lubricated journal bearings. Topics in Fluid Film Bearing and Rotor Bearing System Design and Optimization, ASME, 1978, New York, pp.1-28.
4. Li, D.F., Choy, K.C., and Allaire, P.E. Stability and transient characteristics of four multilobe journal bearing configurations. Trans. ASME, Journal of Lubrication Technology,1980, vol. **102**(3), pp.291-299.
5. Allaire, P.E., Li, D.F., and Choy, K.C. Transient unbalance response of four multilobe journal bearings. Trans. ASME, Journal of Lubrication Technology,1980, vol. **102** (3), pp.300-319.
6. Ghosh, M.K., and Satish, M.R. Rotordynamic characteristics of multilobe hybrid bearings with short sills-part I. Tribology International, 2003, vol. **36**(8), pp. 625–632.
7. Ghosh MK and Satish MR. Stability of multilobe hybrid bearing with short sills—part II. Tribology International, 2003, vol. **36**(8), pp.633–636.
8. Mokhtar, M.O.A, Aly, W.Y., and Shawki, G.S.A. Experimental study of journal bearings with undulating journal surfaces. Tribology International,1984, vol. **17**(1), pp.19–24.
9. Mokhtar, M.O.A, Aly, W.Y., and Shawki, G.S.A. Computer-aided study of journal bearings with undulating surfaces. Journal of Tribology,1984, vol. **106**(4), pp. 468–472.
10. Chennabasavan, T.S., and Raman, R. The effects of geometric irregularities of journals on the performance of porous bearings. J Engineering Tribology,1994, vol. 208, pp.141–145.
11. Sharma, Satish, C., and Rajput, A.K. Effect of geometric imperfections of journal on the performance of micropolar lubricated 4-pocket hybrid journal bearing. Tribology International, 2013, vol. **60**, pp.156-168.
12. Rajput, A.K., and Sharma, Satish, C. A study of capillary-compensated geometrically imperfect six-pocket hybrid journal bearing of various geometric shapes of recess. J Engineering Tribology, 2013, vol. **228**, pp.170–186.
13. Jain, D. and Sharma, S.C. Two-lobe geometrically imperfect hybrid journal bearing operating with power law lubricant. Proceedings of the Institution of Mechanical Engineers, Part J: Journal of Engineering Tribology, 2015, vol. **229**(1), pp.30-46.
14. Tayal, S.P., Sinhasan, R., and Singh, D.V. Analysis of hydrodynamic journal bearing with non-Newtonian power law lubricants by the Finite Element Method. Wear, 1981, vol. **71**, pp.15-27.
15. Safar, Z. S. Journal bearings operating with non-newtonian lubricant films. Wear, 1979, vol. **53**(1), pp. 95-100.

BEHAVIOUR OF INFINITELY SHORT ROUGH BEARING

P.L. Thakkar[1], H.C. Patel[2] and G.M. Deheri[3]

[1]Department of Mathematics, L. D. College of Engineering, Ahmedabad, Gujarat, India
[2]Department of Mathematics, L. D. College of Engineering, Ahmedabad, Gujarat, India
[3]Department of Mathematics, S. P. University, Vallabh Vidhayanagar, Gujarat, India
*Corresponding Author (Email: pragnesh83@gmail.com)

Key words : Journal Bearing, Pressure Distribution, Reynold's Equation, Roughness, Load carrying capacity, friction

ABSTRACT

This paper aims to analyze the performance characteristic of an infinitely short rough bearing. The roughness is modeled in the light of the method of Christensen and Tonder. The stochastically averaged Reynold's equation is solved to get the pressure distribution, load carrying capacity and friction. It is established that the transverse surface roughness affects the system adversely. In addition the friction is found to be increased. In this type of roughness pattern the standard deviation plays a crucial role.

INTRODUCTION

Journal bearings are used to carry radial loads, for example, to support a rotating shaft. A simple journal bearing consists of two rigid cylinders. The outer cylinder (bearing) wraps the inner rotating journal (shaft). Normally, the position of the journal center is eccentric with the bearing center. A lubricant fills the small annular gap or clearance space between the journal and the bearing. The eccentricity of the journal is related to the pressure that will be generated in the bearing to balance the radial load. The lubricant is supplied through a hole or a groove and may or may not extend all around the journal. The need of a Maintenance Free Bearings (MFB) was established by Hirani [1]. The paper presented preliminary friction calculations to highlight the ways to achieve maintenance free bearings. The existing technologies of well-established maintenance free bearings were described. The hybridization of bearing technologies to achieve low cost maintenance free bearings had been exemplified. Finally a combination of passive magnetic repulsion and hydrodynamics had been proposed and recommended as source terms to develop maintenance free bearings. In Raghavendra et al.[2] The analysis and design of hydrodynamic journal bearings has drawn a considerance attention of engineers. Emphasis was given to design those bearings so as to avoid metal-to-metal contact .To design these elements, few important characteristics, like load-carrying capacity, maximum pressure and their location lubricant flow requirement between mating surfaces and so on were to be predicted accurately. These parameters could be determined if the pressure within the clearance space between contact surfaces was known. To study and find this pressure one had to solve in general the Reynolds's equation that governed the flow of lubricant inside the clearance space. Moreover the accuracy of the results obtained by FEM was mainly depended on the proper finite element modeling that included proper selection of the type and size of finite elements and solution algorithm. One was required to determine the minimum number of elements those could be used to obtain the accurate solution. Therefore, this work was devoted to study the effect of number of finite elements on the computed results of hydrodynamic journal bearing and to determine minimum number of finite elements to be used in the analysis of the journal bearing. Dwivedi et al.[3] considered solution of Reynolds equation for hydrodynamic journal bearing with infinitely long approximation, infinitely short bearing approximation and finite journal bearing approximation. Further Finite Journal bearing approximation considers two dimensional solution of Reynolds equation with natural boundary condition, which could not be solved by analytical method. So, here the solutions for finite journal bearing was obtained using finite difference method to get bearing performance parameters such as load capacity and Sommerfeld number etc. by Sandeep Vakharia [4] the steady state performance analysis of short circular journal bearing was conducted using the viscosity correction model under thin film lubrication conditions. The thickness of adsorbed molecular layers was the most critical factor in studying thin film lubrication and was the most essential parameter that distinguished thin film from thick film lubrication analysis. The interaction between the lubricant and the surface within a very narrow gap was considered. The general Reynolds equation was derived for calculating thin film lubrication parameters affecting the performance of short circular journal bearing. Investigation for the load carrying capacity, friction force, torque, and power loss for the short circular journal bearing under the consideration of adsorbed layer thickness had been carried out. The analysis was carried out for the short bearing approximation (L / D = 0.5) using Gumbel's boundary condition. It was found that the steady state performance parameters were comparatively higher for short circular journal bearing under the consideration of adsorbed layer thickness than for plain circular journal bearing.

Numerical continuation was used by Amamou et al.[5] to predict the branch of the journal equilibrium point, the Hopf bifurcation point and the emerging stable or unstable limit cycles. Depending on the bearing characteristics, the stability threshold occurred either at a supercritical or at a subcritical Hopf bifurcation. For journal speeds above the supercritical bifurcation, the journal underwent stable limit cycles. For the stability boundaries due to a subcritical bifurcation, a limit point of cycle bifurcation was found defining the domain of possible journal jumping from the equilibrium position to large limit cycles and hysteresis phenomenon during rotor speed variation near the stability threshold.

Incorporation of different shapes of textures on journal and/or bearing at different location of texture zone was reported by Singh et. al[6]to have significant influence on the bearing performance. Different types of surface roughness / texturing had been proposed and evaluated for this purpose. Constraints were imposed on the maximum fluid pressure, minimum film thickness, maximum temperature rise and critical speed. The Reynolds equation for the pressure distribution of the lubricant in a journal bearing with finite length was solved by Sfyris and Chasalevris[7] analytically. Using the method of separation of variables in an additive and a multiplicative form, a set of particular solutions of the Reynolds equation was added in the general solution of the homogenous Reynolds equation. Thus a closed form expression for the definition of the lubricant pressure was presented. The Reynolds equation was split into four linear ordinary differential equations of second order with variable coefficients. The resultant pressure distribution presented slight differences compared to this of the numerical solution and the approximate analytical solution in the values of maximum and minimum pressure but also in the domain of lower values of pressure. Hence it has been proposed to study and analyze the effect of certain type of roughness on the performance characteristics of a infinitely short rough hydrodynamic journal bearing. The geometry of the bearing system and equilibrium of forces on fluid element are presented in figures 1(a) and 1(b).

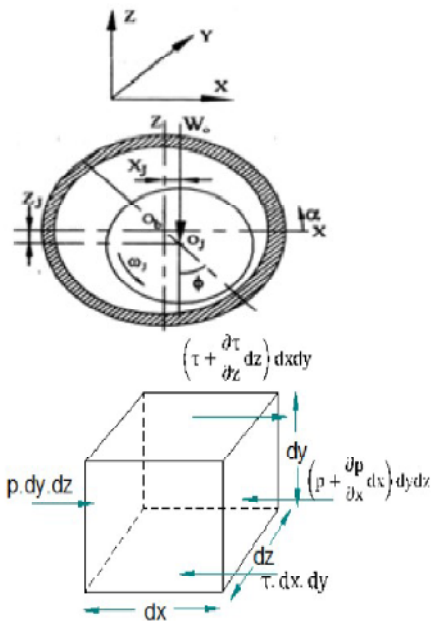

Fig: 1(a) Geometry and Coordinate system
Fig: 1(b) Equilibrium of Forces on Fluid Element

Normal forces due to fluid pressure p act upon the left and right surfaces of the fluid element whereas shear forces due to viscosity act upon the bottom and top surfaces of the fluid element. Considering equilibrium of forces in X-direction, one finds that

$$pdydz + (\tau_x + \frac{\partial \tau_x}{\partial y}dy)dxdz - \tau_x dxdz - (p + \frac{\partial p}{\partial x}dx)dydz = 0$$

$$\therefore \frac{\partial \tau_x}{\partial y} = \frac{\partial p}{\partial x} \qquad (1)$$

According to the Newton‘s law of viscosity

$$\tau_x = \mu \frac{\partial u}{\partial y}$$

Substituting the value in equation (1), one obtains that

$$\frac{\partial p}{\partial x} = \mu \frac{\partial^2 u}{\partial y^2} \qquad (2)$$

this gives pressure gradient in X-direction. Since the pressure of the lubricant is constant in the direction of film thickness that is $\frac{\partial p}{\partial y} = 0$

While the pressure gradient in z direction is $\frac{\partial p}{\partial z} = \mu \frac{\partial^2 w}{\partial y^2}$

For time being we will restrict to analysis in X-direction only. From equation Integrating equation (2) twice with respect to y, this results in

$$u = \frac{1}{2\mu}\frac{\partial p}{\partial x} y^2 + C_1 y + C_2 \qquad (3)$$

The constants of integrations are C_1 and C_2 are evaluated from the following boundary conditions:

$y = 0$ $\qquad$ $u = 0$

$y = h$ $\qquad$ $u = U$

Where U is the velocity in X-direction. In view of boundary conditions one arrives at

$$u = \frac{1}{2\mu}\frac{\partial p}{\partial x}(y^2 - hy) + \frac{U}{h}y \qquad (4)$$

Thus equation gives the velocity distribution of Lubricant in the film as a function of y and $\frac{\partial p}{\partial x}$ pressure gradient

The flow rate of lubricant in X-direction per unit width of Z-direction is given by

$$q_x = \int_0^h u\, dy = -\frac{h^3}{12\mu}\frac{\partial p}{\partial x} + \frac{Uh}{2} \tag{5}$$

Similarly, the flow rate of lubricant in the Z-direction per unit width of X-direction is found

$$q_z = -\frac{h^3}{12\mu}\frac{\partial p}{\partial z} + \frac{Wh}{2} \tag{6}$$

Assuming there is no flow of lubricant in the Y-direction, the Reynolds's equation is obtained as

$$\frac{\partial}{\partial x}\left[\frac{h^3}{\mu}\frac{\partial p}{\partial x}\right] + \frac{\partial}{\partial z}\left[\frac{h^3}{\mu}\frac{\partial p}{\partial z}\right] = 6\left[\frac{\partial}{\partial x}(Uh) + \frac{\partial}{\partial z}(Wh)\right] \tag{7}$$

As U and W are not a function of x and z respectively.

It is, in fact very hard to think of any moving system where wedge h vary in two dimensions i.e. X and Y. Hence consideration of $\frac{\partial p}{\partial x} = 0$.

$$\frac{\partial}{\partial x}\left[h^3\frac{\partial p}{\partial x}\right] + \frac{\partial}{\partial z}\left[h^3\frac{\partial p}{\partial z}\right] = 6\mu U\frac{dh}{dx} \tag{8}$$

The pressure distribution along circumference is shown in figure

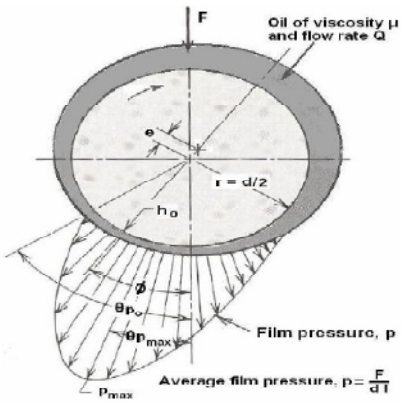

Fig. 2(a) : Pressure distribution along circumference

Pressure Distribution

For infinitely short journal bearing

$$\frac{\partial p}{\partial x} = 0 \tag{9}$$

Substituting equation (9) in equation (8)

$$\frac{\partial}{\partial z}\left[h^3\frac{\partial p}{\partial z}\right] = 6\mu U\left[\frac{dh}{dx}\right] \tag{10}$$

In view of discussion of Christensen and Tonder [8-10] this leads

$$\frac{\partial}{\partial z}\left[(h^3+3\sigma^2h)\frac{\partial p}{\partial z}\right] = 6\mu U\left[\frac{d}{dx}(h^3+3\sigma^2h)^{\frac{1}{3}}\right] \tag{11}$$

Fluid film thickness h is not a function of z, hence equation (10) becomes

$$\frac{d^2p}{dz^2} = \frac{6\mu U}{(h^3+3\sigma^2h)}\frac{d}{dx}\left(h^3+3\sigma^2h\right)^{\frac{1}{3}} \tag{12}$$

Integrating above equation

$$p = \frac{3\mu U}{(h^3+3\sigma^2h)}\frac{d}{dx}\left(h^3+3\sigma^2h\right)^{\frac{1}{3}}z^2 + c_1z + c_2 \ldots\ldots \tag{13}$$

Using the boundary conditions

$$z = \pm\, l/2 \qquad p = 0$$

$$z = 0 \qquad \frac{dp}{dz} = 0$$

and simplifying, one gets the expression for pressure distribution in the bearing system as

$$p = \frac{3\mu Ul^2}{c^2r}\frac{(\varepsilon\sin\theta)\left[(1+\varepsilon\cos\theta)^2+\frac{\sigma^2}{c^2}\right]}{\left[(1+\varepsilon\cos\theta)^3+3\frac{\sigma^2}{c^2}(1+\varepsilon\cos\theta)\right]^{\frac{5}{3}}}\left[\frac{1}{4}-\frac{z^2}{l^2}\right] \tag{14}$$

Introduction of dimensionless quantities

$$\sigma^* = \frac{\sigma}{c} \qquad z^* = \frac{z}{l} \qquad P = -\frac{c^2r}{\mu Ul^2}p$$

Leads to the expression for the pressure distribution in the dimensionless form

$$P = \frac{(3\varepsilon\sin\theta)\left[(1+\varepsilon\cos\theta)^2+\sigma^{*2}\right]}{\left[(1+\varepsilon\cos\theta)^3+3\sigma^{*2}(1+\varepsilon\cos\theta)\right]^{\frac{5}{3}}}\left[\frac{1}{4}-z^{*2}\right] \tag{15}$$

Load carrying capacity

By using pressure distribution the load carrying capacity of the bearing can be obtained. The load carrying capacity is determined by using half Sommerfeld condition. Cameron [11]. The half Sommerfeld condition states that when the film becomes divergent at $\theta = \pi$ the pressure becomes zero. Hence only the positive pressure region that is convergent film region $\theta = 0$ to $\theta = \pi$ supports the total load in bearing.

The component of total force in the direction of line of centres (N-direction) is described by,

$$W_N = \int_0^{\pi} \int_{-l/2}^{l/2} p\, r\, d\theta\, dz \cos\theta \tag{16}$$

The component of total force in the direction of line of centres (T-direction) is given by,

$$W_T = \int_0^{\pi} \int_{-l/2}^{l/2} p\, r\, d\theta\, dz \sin\theta \tag{17}$$

Load Carrying capacity of the bearing is given by

$$W = \sqrt{W_N^{\,2} + W_T^{\,2}} \tag{18}$$

Resulting load carrying capacity is computed by Trapezoidal rule.

Friction

The friction force is determined by

$$f = \int_0^{2\pi} \frac{\mu U}{h^3 + 3\sigma^2 h} L\, R\, d\theta \tag{19}$$

which turns out to be governed by the expression

$$f = \frac{\mu U L^3 r}{c^3 L^2} \int_0^{2\pi} \frac{1}{c^3(1+\varepsilon\cos\theta)^3 + 3\sigma^2 c(1+\varepsilon\cos\theta)} d\theta \tag{20}$$

Non dimensional frictional force is given by

$$F = \frac{fc^3}{\mu U L^2 r} = \frac{1}{L^2} \int_0^{2\pi} \frac{1}{c^3(1+\varepsilon\cos\theta)^3 + 3\sigma^2 c(1+\varepsilon\cos\theta)} d\theta \tag{21}$$

Also the coefficient of friction is decided by the relation

$$\mu = \frac{F}{W}$$

The performance characteristics W, f, F and μ are calculated by adopting Trapezoidal rule.

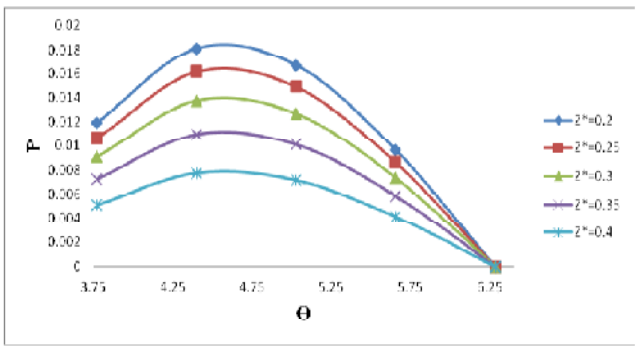

*Fig. 3: Non dimensional pressure distribution P versus θ for different value of z**

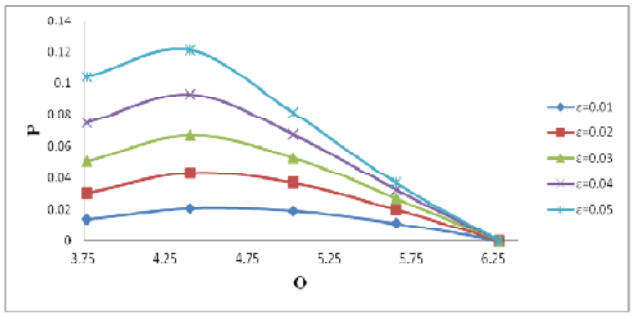

Fig. 4: Non dimensional pressure distribution P versus θ for different value of ε

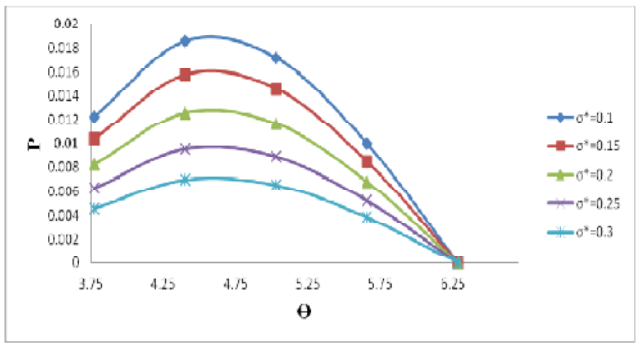

*Fig. 5: Non dimensional pressure distribution P versus θ for different value of σ**

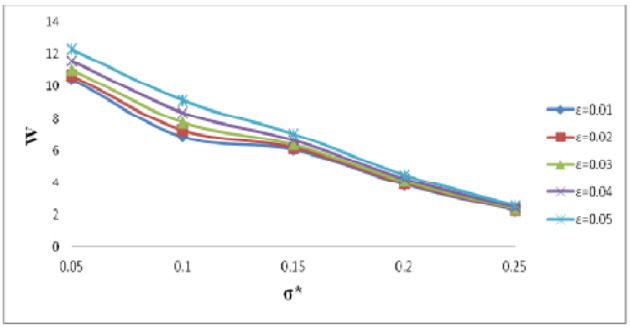

Fig. 6: Non dimensional load carrying capacity w versus σ for different values of ε*

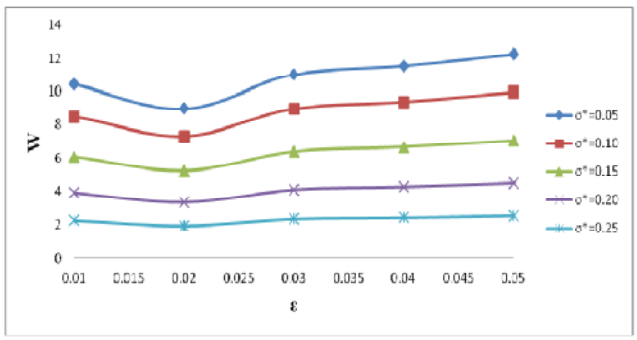

*Fig. 7: Non dimensional load carrying capacity w versus ε for different values of σ**

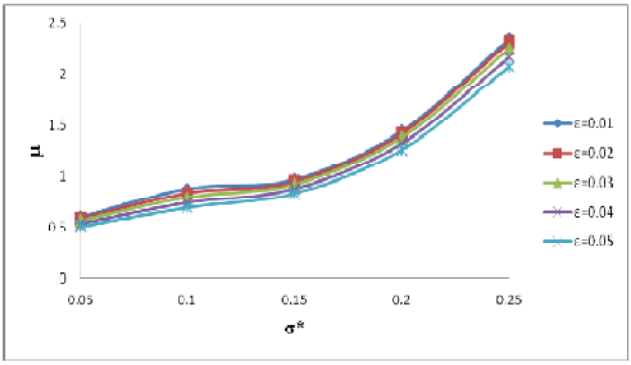

Fig. 8: Coefficient of friction μ versus σ^* for different values of ε

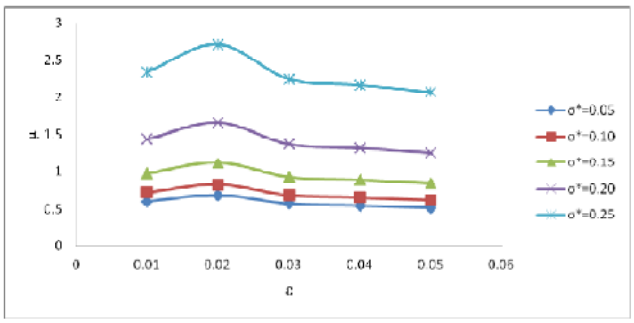

Fig. 9: Coefficient of friction μ versus σ^* for different values of ε

RESULT AND DISCUSSION

The nerely parabolic profile of the pressure distribution can be seen from fig 3,4 and 5.However the decresing pressure is littlebit slow in the case of å.The variance of non dimensional load carrying capacity is presented in fig 6 and 7.It is clearly seen that the standard devivation adversely affects the performance of the bearing system.Further the effect of eccentricity on the variance of load carrying capacity with respect to ó* is negligible when ó* exceeds 0.15. The profile for cofficent of friction is provided in fig 8 and 9.It is clear that the standard deviation increses the the cofficent of friction but the affects of skeness on the coefficient of friction with respect to ó* is almost marginal.

CONCLUSION

This article reveles that the performance charactersitics of a infinitely short journal bearing are singificantly affected by the standard devivation associated with the roughness charactersitics.The bearing reffers due to the transeverse surface roughness. So while desiging the bearing system one is requred to account for roughness.

Nomenclature

p: Lubricant pressure (N/mm2)

P: Dimensionless pressure

w: Load-carrying capacity (N)

F: Dimensionless friction force

μ: Coefficient of friction

W: Dimensionless load carrying capacity

h: Lubricant viscosity (N.S/mm2)

e: Eccentricity (mm).

σ: Standard deviation

REFERENCES

1. Muzakkir, S. M., and Harish Hirani. "Maintenance Free Bearings." International Journal of Engineering Research 4.3 (2015): 133-136.
2. Raghavendra, N., M. C. Math, and Pramod R. Sharma. "Finite Element Method Analysis of Hydrodynamic Journal Bearing." European Journal of Advances in Engineering and Technology 2.2 (2015): 92-101.
3. V.K.Dwivedi, S. Chand, K. N. Pandey, "Analysis of Hybrid (Hydrodynamic/Hydrostatic) Journal Bearing", Advanced Materials Research, Vol. **650**, pp. 385-390, Jan. 2013.
4. Sandeep Soni and D. P. Vakharia, "Performance Analysis of Short Journal Bearing under Thin Film Lubrication," ISRN Mechanical Engineering, vol. 2014, Article ID 281021, 8 pages, 2014.
5. Amamou, Amira, and Mnaouar Chouchane. "Nonlinear stability analysis of long hydrodynamic journal bearings using numerical continuation." Mechanism and Machine Theory **72** (2014): 17-24.
6. Singh, Pratibha, et al. "OPTIMUM DESIGN OF JOURNAL BEARING THROUGH SURFACE TEXTURING-A REVIEW." International Journal 2.1 (2014).
7. Sfyris, D., and A. Chasalevris. "An exact analytical solution of the Reynolds equation for the finite journal bearing lubrication." Tribology International 55 (2012): 46-58.
8. Christensen, H., and K. Tonder. "The hydrodynamic lubrication of rough bearing surfaces of finite width." Journal of Tribology 93.3 (1971): 324-329.
9. Christensen, H., and K. Tonder. "The hydrodynamic lubrication of rough journal bearings." Journal of Tribology 95.2 (1973): 166-172.
10. Tønder, K., and H. Christensen. "Waviness and roughness in hydrodynamic lubrication." Proceedings of the Institution of Mechanical Engineers 186.1 (1972): 807-812.
11. CAMERON, A.: Principles of Lubrication, Longman, 1974.

FZG gear test rig

The FZG gear test rig is a test machine with a mechanical power circuit. The drive gearbox and the text gearbox are frictionally engaged by two torque shafts (hereinafter only mentioned as shafts). For load application a clutch is provided on shaft 1. The temperature in the test gearbox can be set and controlled. The test rig is driven by an electric motor. The speed is 1,500 rpm. The variable-speed test rig allows speeds from 100 rpm to 3,000 rpm and two directions of rotation. The load can either be applied by a weight system or a the tension ratchet or with a automatically load system.

Highlights

- Delivered worldwide to more than 200 reputable customers
- Standards: ISO 14635, CEC-L-07, IP 334, ASTM D 5182, ASTM D 4998, FVA 243, FVA 54, FVA 2
- Option: Wear at low speed
- 2 oil units possible
- Siemens control with colour LCS
- Curve display
- Determination of scoring load capacity of oils
- Pitting test to determination the effects of various transmission oils and additives on gears
- Micropittings test to determine the effects of additives and oils on the occurrence of micropittings
- Shear stability test to determine the frictional losses of multi-grade oils

Technical data

- Speed : 100 3,000 rpm
- Two directions of rotation
- Max. torque: 715Nm (pinion)
- Max. oil temperature: 120°C (dip)/90°C (inject)
- Center distance: 91,5mm

Also Available

- Transmission Axle efficiency Test Rig
- Back to Back Planetary Gear Test Rig
- Bearing Test Rig for Turbocharger
- Turbine Wheel / Compressor Wheel Test Rig
- Gear Test Rig for Noise Test
- Clutch Test Rig
- Drive Shaft Test Rig
- Anti-Friction Bearing Test Rig
- Axle Bearing Fatigue Test Rig
- Worm Gear Test Rig
- Bevel Gear Test Rig
- Hypoid Ger Test Rig
- Four Square Gear Test Rig for Fatigue & Strength Testing
- Variable Centre Distance Gear Test Rig
- Endurance Test Rig

STRAMAMPS

Strama-MPS Maschinenbau GmbH & Co. KG
Ittlinger Str. 195 . 94315 Straubing
Product manager FZG Christoph Wolf
christoph.wolf@strama-mps.de
Tel. +49 9421/739-164 . Fax +49 9421/739-200
www.strama-mps.de

For Details Contact :
Tribotech Technologies Pvt. Ltd.
Mobile : +91 9810077557
+91 9810377557
E-mail : ttpl.ttpl@gmail.com